CZECH TECHNICAL UNIVERSITY IN PRAGUE

Faculty of Electrical Engineering

Bachelor thesis

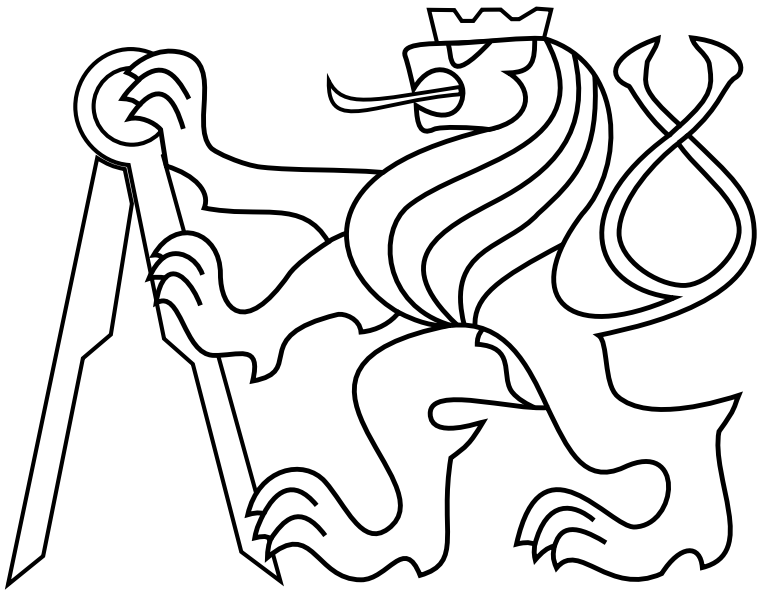

Matouš Vrba

Active Searching of RFID Chips by a Group of Relatively Stabilized Helicopters

Department of Cybernetics

Thesis supervisor: **Dr. Martin Saska**

March, 2016

Prohlášení autora práce

Prohlašuji, že jsem předloženou práci vypracoval samostatně a že jsem uvedl veškeré použité informační zdroje v souladu s Metodickým pokynem o dodržování etických principů při přípravě vysokoškolských závěrečných prací.

V Praze dne ....
podpis autora práce

Author statement for undergraduate thesis

I declare that the presented work was developed independently and that I have listed all sources of information used within it in accordance with the methodical instructions for observing the ethical principles in the preparation of university theses.

Prague, date ....
signature

Czech Technical University in Prague
Faculty of Electrical Engineering

Department of Cybernetics

BACHELOR PROJECT ASSIGNMENT

Student: Matouš V r b a

Study programme: Cybernetics and Robotics

Specialisation: Robotics

Title of Bachelor Project: Active Searching of RFID Chips by a Group of Relatively Stabilized Helicopters

Guidelines:

The aim of the thesis is to design, develop and experimentally verify a method that enables to cooperatively localize RFID chips by a group of Micro Aerial Vehicles (MAVs). The following main tasks will be solved.

- To design and implement a device (transmitter and receiver with SW for measuring signal intensity) for testing possibility of estimation of distance between MAVs and the transmitters deployed in the environment based on cooperative measurement of intensity of their signals.
- To design and implement a method for coverage of an environment by a formation of MAVs and an approach for filtering the information obtained during the initial flight.
- To design and implement an algorithm for adaptive motion planning based on current estimation of positions of transmitters and uncertainty of measurement with the aim to increase reliability of their pose determination.
- To verify the system in robotic simulator V-REP and to prepare it for using with real MAVs.
- To realize a feasibility study of the proposed system based on experiments with statically deployed receivers and a simple experiment with one MAV or several MAVs carrying the receiver.

Bibliography/Sources:

[1] S. J. Julier and J. K. Uhlmann. A New Extension of the Kalman Filter to Nonlinear Systems. In Proc. of AeroSense: The 11th Int. Symp. On Aerospace/Defence Sensing, Simulation and Controls, 1997

[2] J. Rodas, T. M. Fernandez, D. I. Iglesia, C. J. Escudero. Multiple Antennas Bluetooth System for RSSI Stabilization, in Wireless Communication Systems, 2007.

[3] T. M. Bielawa. Position Location of Remote Bluetooth Devices. Blacksburg, VA, USA. Master's thesis. Virginia Polytechnic Institute and State University, 2005.

[4] T. Krajnik, M. Nitsche, J. Faigl, P. Vanek, M. Saska, L. Preucil, T. Duckett and M. Mejail. A Practical Multirobot Localization System. Journal of Intelligent & Robotic Systems 76(3-4):539-562, 2014.

Bachelor Project Supervisor: Ing. Martin Saska, Dr. rer. nat.

Valid until: the end of the summer semester of academic year 2016/2017

L.S.

prof. Dr. Ing. Jan Kybic
Head of Department

prof. Ing. Pavel Ripka, CSc.
Dean

Prague, January 14, 2016

Acknowledgements

I would like to thank my supervisor Martin Saska for his help and guidance throughout this thesis. I would also like to thank Vojtěch Spurný, Tomáš Báča, Lukáš Vojtěch and Marek Nedura for their help with specific problems I encountered during my work on this thesis and with the experiments. Finally, I would like to thank my family for their help, support and guidance in my life.

Abstract

A novel solution to the problem of localizing RF transmitters is presented in this thesis. Target application is the ability to find an object, which has been tagged with a transmitter, in a desired area, where the GPS may be unavailable or when better precision is required. It may find use for example in finding soldiers in the field, cars in urban areas, tools in construction sites, animals, etc. Contemporary methods for localizing RF transmitters are usually based on creating a map of RSSI values in an area beforehand and then comparing it to the measurements when localizing to find the best matching position, or less frequently on trilateration from some form of distance measurements. They mostly rely on stationary receivers placed in the area and generally require time consuming setup and preparation. The presented solution utilizes a formation of MAVs (Micro Aerial Vehicles), carrying RF receivers, to scout the area for transmitters and report their positions. It is based on the Kalman Filter and relies on measuring RSSI with the MAVs at different positions in the area. The precision and robustness of the algorithm is on the same level with state-of-the-art localization algorithms, however, the new proposed algorithm does not require any preinstalled infrastructure, which makes it much easier and cheaper to implement in a variety of locations.

Keywords: micro aerial vehicle, radio frequency identification, Kalman Filter, Bluetooth Low Energy, localization

Abstrakt

V této práci je představeno nové řešení problému lokalizace RF vysílačů. Cílovou aplikací je hledání objektu, který byl označen vysílačem, v dané oblasti, kde je GPS nedostupná nebo když je vyžadována vyšší přesnost lokalizace. Využití může nalézt například pro vyhledávání vojáků na bojišti, aut v zastavěných oblastech, nástrojů na staveništích, zvířat apod. Současné metody vyhledávání RF vysílaču jsou obvykle založeny na vytvoření mapy hodnot RSSI v této oblasti předem, a následném porovnávání RSSI měření při lokalizaci s touto mapou pro nalezení polohy s nejlépe odpovídající hodnotou. Další metody jsou založeny například na trilateraci polohy ze vzdáleností mezi vysílači a přijímači, které mohou být měřeny různými způsoby. Všechny tyto metody ale většinou využívají stacionární přijímače rozmístěné v oblasti a obecně vyžadují časově náročné přípravy. Řešení, prezentované v této práci, využívá k vyhledávání vysílačů v oblasti formaci bezpilotních helikoptér, nesoucích RF přijímače. Je založeno na měření RSSI v různých místech v oblasti pomocí těchto helikoptér a na Kalmanově Filtru. Simulace a experimenty, které jsou popsané v této práci, ukazují, že navrhovaný algoritmus je použitelný pro cílovou aplikaci a že co do přesnosti a robustnosti může konkurovat ostatním současným lokalizačním algoritmům bez toho, aby vyžadoval předpřipravenou infrastrukturu.

Klíčová slova: bezpilotní helikoptéra, radio frequency identification, Kalmanův Filtr, Bluetooth Low Energy, lokalizace

Contents

List of Figures

1 Introduction

With the mobile robotics being on the rise in many different fields, new possibilities and new uses arise. Mobile robots and especially micro aerial vehicles (MAVs) are used more frequently in industry, military, arts or simply as a hobby. Applications range from inspecting the power grid cables, remotely fighting an enemy, taking dynamic photos and filming movies, to flying just for the joy of it. As the tablets and cell phones industry grows bigger, demand for cheap and power-economic yet still capable processors, graphical processing units, transmitters and other devices grows as well. This brings new technologies to satisfy these demands to the market. These devices are not suitable only for consumer electronics, but can be utilised in mobile robotics as well.

Applying these new technologies, new applications can easily be derived, such as using a formation of mobile robots to scout an area for transmitters and report their positions, which is tackled in this thesis. Thanks to their versatility, high mobility, ability to navigate easily even in difficult terrain and their ability to change altitude, MAVs seem ideal for this task. This approach could not be realised without new advances in technology since the required computer vision, control and filtering algorithms are too computationally intensive for classic microcontrollers and older processors are too heavy and power inefficient to run on an MAV. The specific target of this application is the ability to find an item, which has been tagged with an unobtrusive and long lasting beacon (transmitter), in a relatively large area. The localization is done with a formation of MAVs carrying receivers, and without the need for any infrastructure to be present. This work builds on latest achievements in the field of path following in a formation [1], [2], which are used for finding a stable and reliable way to wirelessly locate a beacon in direct line of sight utilizing radio transmission.

There are multiple possible approaches to the problem of finding a beacon position relatively to known positions of one or more receivers. Standard approaches use information about distance or angle from the receivers to the beacon and analytically compute the relative position through some of the several possible combinations of this geometrical problem [3], [4]. These are mostly simplified to a two dimensional problem. There are different technologies to measure the angle or distance with variable levels of complexity, reliability, power requirements and price, for example ultrasonic based methods [5] or radio frequency methods based on signal strength or time of flight [3], [6]. For this work, the new Bluetooth 4.0 (BLE) specification has been chosen as the radio transmitter/receiver technology. It is designed to be low-power, cheap, simple to interface and widely available. The downside is that there is no direct way to measure distance and no simple way to measure angle between two devices. Even though the distance can be calculated from RSSI (Received Signal Strength Indicator) values, the Bluetooth specification was not designed for this kind of operation and the results are not very accurate without additional processing (see sections 5.1 and 5.2 for plots of RSSI measurements over distance). The standard geometrical approaches are therefore unstable and often have no solution. That is why a more complex approach had to be embraced.

To make up for the low stability and accuracy of the input, a variant of the Kalman Filter has been used, specifically a generalization of the Kalman Filter for non-linear systems called Extended Kalman Filter (EKF). Similarly as the Kalman Filter, it offers iterative state estimation and input filtering, it works with two stages of prediction and update and its output is a state estimation and a state covariance matrix. It uses a first order linearisation of the non-linear system model. A more in-depth description is provided for example in [7] or [8].

This thesis is built upon previous research conducted at the Czech Technical University in Prague, Department of Cybernetics, dealing with the path following and formation control problems [9]. The path following problem has been solved in previous work [10] (an article about this work: [11]). It implements an MPC control algorithm on a custom MAV platform. The MAV carries a *px4flow*[1] sensor for measuring height and velocity of the MAV and a *KK2*[2] board to provide basic stabilization in combination with a custom designed control board, running the MPC. The formation control problem has been solved in previous work [12]. It has been implemented on MAV onboard computers. The MAVs carry identification patterns and cameras. The targets are localized using the cameras and computer vision with an algorithm, described in [13]. This information is then used to correct the setpoints for the MPC control algorithm and hold the formation [2]. The onboard variant of the system for relative localization of members of multi-MAV teams is described in [14] with examples of its deployment in [15] and [16]. This work has been a source of information for this thesis and although the formation control has not been utilized here, it will be useful in further development. A photo of one of the MAVs with this hardware and software setup, which has been used in this thesis, can be seen on Figure 1. A photo of two MAVs with the identification patterns can be seen of Figure 2.

1.1 Related work

Localization using wireless technology is a widely used concept. Systems like the GPS, radars, or WiFi triangulation based methods are commonly used. Positioning systems using Bluetooth exist as well (for example the *ZONITH*[3] or *Spreo*[4] indoor positioning systems). Most of the Bluetooth based systems focus on indoor localization using a prepared infrastructure of static devices meant to track moving devices. These systems sometimes use RSSI values for distance calculation and then trilateration to calculate position, or ecolocation to determine in which area the device is. Probably the mostly used method in actual research and in applications is fingerprinting of certain locations with their corresponding RSSI values and then choosing the best fitting location based on current measurements [3], [17], [18]. This method requires time consuming setup and calibration as the RSSI

[1] See `https://pixhawk.org/modules/px4flow`

[2] From `http://www.hobbyking.com`

[3] See `http://zonith.com/products/rtls/`

[4] See `http://spreo.co/products/indoor-positioning-systems/`

values need to be measured at the desired locations beforehand. According to [17], the fingerprinting approach with Bluetooth technology had a precision with 50% probability of being within 1.5 m of the actual position when the localized device does not move. The best result from [18], which used fingerprinting and WiFi, had a mean error of 1.21feet = 0.37 m for a moving target, but with the tendency to "get lost" and integrate a large error over time, or 1.10 m without "getting lost". These systems might require recalibration when some environmental conditions like humidity, temperature or obstacles in the area change [6]. This problem has been addressed in [6], where a self-calibrating approach based on measurements of WiFi RSSI has been proposed, which achieved a mean error of 1.84 m with six WiFi APs on an area of 600 m^2. The work, presented in this paper, focuses on a situation where no preinstalled infrastructure is present and therefore these methods can only be used either with modifications or not at all. Best experimental results, achieved with the proposed algorithm, were localizing a static beacon with resulting error of 0.28 m and tracking a moving beacon for one minute with a mean error of 1.37 m. The simulation suggests that in conditions closer to optimal (described in section 4) an average localization error of static beacons could be as small as 0.24 m. The precision of this approach and no need for preinstalled infrastructure are the main contributions of this work.

The method deployed in this work makes use of calculating distance from Bluetooth RSSI measurements. There is existing research regarding this problem. A comprehensive overview of distance measurements using Bluetooth (including RSSI) and also experiments measuring the influence of relative antennae orientation on the RSSI are presented in [3]. In section 3 of [4] the author compares different means of distance measurement using Bluetooth and generally comes to a conclusion that RSSI is the most appropriate. In [19] the authors explore the possibility to use an array of antennae to amplify the measurement precision. A similar approach could be used to increase the RSSI measurement precision in future developments of this work as well. These works have been useful in pointing out the difficulties of implementing distance measurement using Bluetooth and RSSI.

The Kalman Filter is used in the presented algorithm for data fusion from multiple sensors, filtering and state estimation. The two main variants of the KF for nonlinear systems are Unscented Kalman Filter and Extended Kalman Filter. The EKF is older and generally well understood. It uses a linearization of the system model. The UKF uses a novel approach of propagating sigma-points, generated with an unscented transform, through the non-linearities to achieve better precision [20]. There are several studies comparing the two approaches. [21] provides a comprehensive study, comparing different filtering and sensor fusion techniques including the first order EKF and the UKF and concluding that the UKF is better suited for strongly nonlinear systems. Similarly, [22] comes to a conclusion that the UKF performs slightly better than the EKF, based on experimental results from both indoor and outdoor wireless localization. For quasi-linear systems the UKF may give comparable results at the cost of higher computational intensity when compared to the simpler EKF [7], [8]. In this thesis, simulation has been done to determine which variant of the KF fits better for the tackled problem and system setup (section 4).

1.2 Problem statement

The system setup consists of three MAVs and a given number of self-sufficient stationary beacons. The target scenario is to locate the beacons. Each MAV carries one receiver capable of measuring the RSS (received signal strength). Each beacon is equipped with an identifiable transmitter (with a unique ID), compatible with the receivers. The number of beacons together with their IDs is assumed to be known a priori. The beacons are scattered across a flat area free of obstacles. The area is specified as a rectangle, relatively to the MAVs starting position. The MAVs are localized relatively to each other (moving in a known formation) and also to the starting point in a global coordinate system.

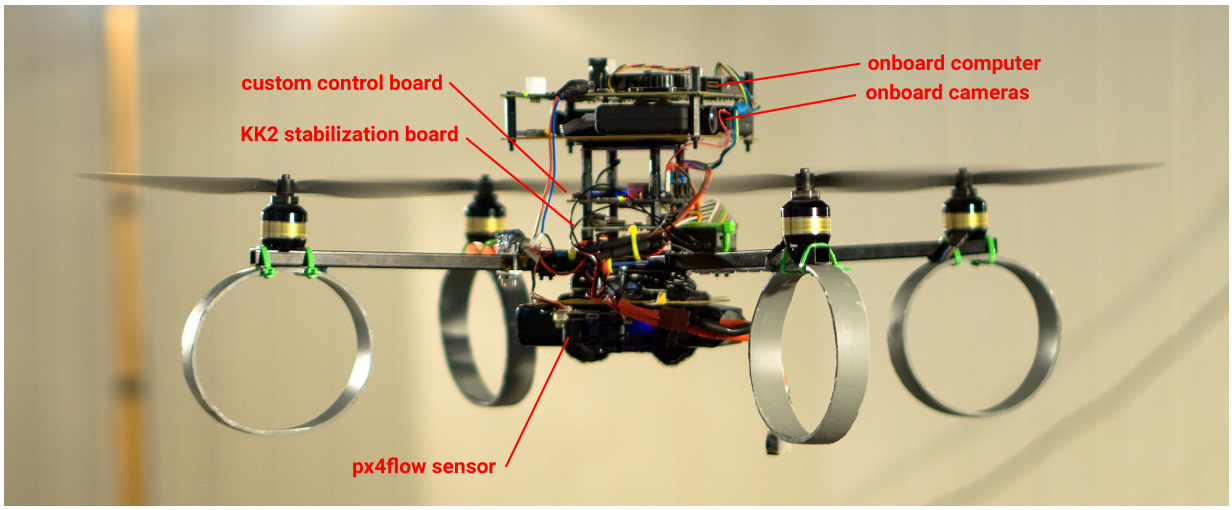

Figure 1: Photo of an MAV, used for experiments in this thesis

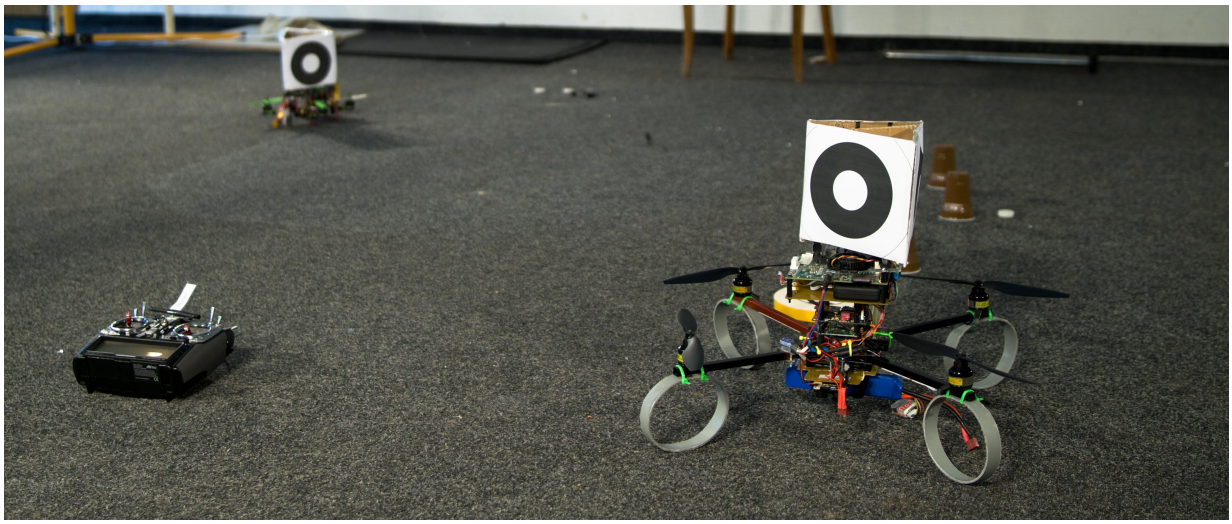

Figure 2: Photo of MAVs with paper targets, used for experiments in this thesis

2 System model

This section describes a model of the system of M MAVs and one beacon. In case localization of multiple beacons is required, the same system model is applied to each of them. The model is constructed in a three dimensional cartesian coordinate system. It can be simplified to two dimensions by trimming the states corresponding to the z coordinate (as was done in the simulations).

Parameters determining the system properties, described in detail in this section, are listed in Table 1. Variables used when describing the system are listed in Table 2. A notation $r \times c$ is used in this work to describe matrix sizes, where r is the number of rows and c is the number of columns.

The system can be generally described using a non-linear discrete state-space model

$$\vec{x}[k+1] = \vec{f}(\vec{x}[k], \vec{u}[k], \vec{v}[k], k), \tag{1}$$
$$\vec{z}[k] = \vec{h}(\vec{x}[k], \vec{u}[k], \vec{w}[k], k). \tag{2}$$

Specifically, the system considered here can be described using a simplified variant of this model

$$\vec{x}[k+1] = \mathbf{A}\vec{x}[k] + \mathbf{B}\vec{u}[k] + \vec{v}[k], \tag{3}$$
$$\vec{z}[k] = \vec{h}(\vec{x}[k]) + \vec{w}[k]. \tag{4}$$

The states, measured values and inputs of the system have been defined using the variables from Table 2 as

$$\vec{x}[k] = \begin{bmatrix} x_1[k], & y_1[k], & z_1[k], & \dots, & x_M[k], & y_M[k], & z_M[k], & x_b[k], & y_b[k], & z_b[k] \end{bmatrix}^T,$$
$$\vec{z}[k] = \begin{bmatrix} \tilde{x}_1[k], & \tilde{y}_1[k], & \tilde{z}_1[k], & \dots, & \tilde{x}_M[k], & \tilde{y}_M[k], & \tilde{z}_M[k], & s_1[k], & \dots & , & s_M[k] \end{bmatrix}^T,$$
$$\vec{u}[k] = \begin{bmatrix} {}_\Delta x_1[k], & {}_\Delta y_1[k], & {}_\Delta z_1[k], & \dots, & {}_\Delta x_M[k], & {}_\Delta y_M[k], & {}_\Delta z_M[k] \end{bmatrix}^T,$$

and the matrices $\mathbf{A}$ and $\mathbf{B}$ as

$$\mathbf{A} = \mathbf{I}_{3(M+1)\times 3(M+1)}, \qquad \mathbf{B} = \begin{pmatrix} \mathbf{I}_{3M\times 3M} \\ \mathbf{0}_{3\times 3M} \end{pmatrix}.$$

In the function $\vec{h}(\vec{x}[k])$, the first $3M$ components are measurements of the first $3M$ states, corresponding to the MAV coordinates. The remaining 3 measurements are formulated

using the Log-Normal model (which is described in Section 2.1):

$$\vec{h}(\vec{x}[k]) = \begin{bmatrix} x_1[k] \\ y_1[k] \\ z_1[k] \\ \vdots \\ x_M[k] \\ y_M[k] \\ z_M[k] \\ P_{0,1} - 10n_1 \log_{10}\left(\sqrt{(x_1[k]-x_b[k])^2 + (y_1[k]-y_b[k])^2 + (z_1[k]-z_b[k])^2}\right) \\ \vdots \\ P_{0,M} - 10n_M \log_{10}\left(\sqrt{(x_M[k]-x_b[k])^2 + (y_M[k]-y_b[k])^2 + (z_M[k]-z_b[k])^2}\right) \end{bmatrix},$$

where parameters $P_{0,i}$ and n_i correspond to the receiver on the i-th MAV. Their meaning is explained in section 2.1. They have to be determined experimentally, which is described in section 2.2.

The random variables $\vec{v}[k]$ and $\vec{w}[k]$ are column vectors of length $3(M+1)$ and $4M$. They are presumed to have a gaussian distribution with zero mean and covariance matrices $\mathbf{Q}$ and $\mathbf{R}$ with sizes $3(M+1) \times 3(M+1)$ and $4M \times 4M$, respectively. The state covariance matrix $\mathbf{P}[k]$, which is generated by the KF, has a size $3(M+1) \times 3(M+1)$.

Parameter	Meaning
M	number of MAVs
$\mathbf{A}, \mathbf{B}, \vec{h}(\vec{x}[k])$	parameters used for state space model description
$\mathbf{Q}$	process noise covariance matrix
$\mathbf{R}$	measurement noise covariance matrix
$P_{0,i}$	received power of the i-th receiver at distance of 1 m
n_i	loss factor of the received power

Table 1: System parameters

Variable	Meaning
$k \in \{0, 1, \ldots, k_{end}\}$	time index
$i \in \{1, 2, \ldots, M\}$	marks variables related to the i-th MAV
$\vec{z}[k]$	vector of measured variables at time step k
$\vec{x}[k]$	vector of system states estimated by the KF
$\vec{u}[k]$	vector of system inputs
$\mathbf{P}[k]$	state covariance matrix
$\vec{v}[k] \sim \mathcal{N}(\mathbf{0}, \mathbf{Q})$	random vector representing process noise
$\vec{w}[k] \sim \mathcal{N}(\mathbf{0}, \mathbf{R})$	random vector representing measurement noise
$\vec{p}_i[k] \equiv \begin{bmatrix} x_i[k], & y_i[k], & z_i[k] \end{bmatrix}$	i-th MAV position in the global coordinate system
$\vec{p}_b[k] \equiv \begin{bmatrix} x_b[k], & y_b[k], & z_b[k] \end{bmatrix}$	beacon position in the global coordinate system
$s_i[k]$	RSSI measurement of the i-th MAV
$\tilde{\vec{p}}_i[k] \equiv \begin{bmatrix} \tilde{x}_i[k], & \tilde{y}_i[k], & \tilde{z}_i[k] \end{bmatrix}$	measurement of the i-th MAV position
${}_\Delta\vec{p}_i[k] \equiv \begin{bmatrix} {}_\Delta x_i[k], & {}_\Delta y_i[k], & {}_\Delta z_i[k] \end{bmatrix}$	$\tilde{\vec{p}}_i[k] - \vec{p}_i[k-1]$

Table 2: System variables

2.1 Received signal strength model

The Log-Normal model has been used to model the signal transmission characteristics. It is a generalized form of the Friis transmission equation, which describes transmission of a radio frequency signal under certain idealized conditions. The Friis transmission equation can be formulated for decibels as

$$P_r = P_t + G_t + G_r + 20 \log_{10} \left(\frac{\lambda}{4\pi R} \right), \tag{5}$$

where P_r, G_r, P_t and G_t are the received power, receiver antenna gain, transmitted power and transmitter antenna gain, respectively. G_t and G_r are in decibels, P_t and P_r are in decibel milliwatts. λ is the wavelength (in meters), corresponding to the radio frequency, and R is distance between the transmitter and receiver antennae (also in meters).

One of the assumed idealized conditions is certainly not met under the working conditions - that the transmitter and receiver are in free space with no signal reflections. It is difficult to determine some of the parameters of the formula. For example, the antenna gains are dependant not only on the hardware, but also on software implementation of the bluetooth driver, which can vary. This model also doesn't account for random noise due to electrical and radio interferences or noise from other sources. To consider these imperfections, the model can be used in the so-called Log-Normal form as

$$\begin{aligned} P_r = P_0 - 10n \log_{10}(R) + \chi, \\ \chi \sim \mathcal{N}\left(\mu_\chi, \sigma_\chi^2\right), \end{aligned} \tag{6}$$

where P_r is again the received power, P_0 and n are parameters, which can easily be calibrated (more on this in Section 2.2), and R is the distance between transmitter and receiver. χ is a gaussian random variable with mean μ_χ and variance σ_χ^2. It represents the model uncertainty and noise. In case of the localization algorithm, the mean is presumed equal to zero. Note that using this model the random variable representing noise is additive, which is also why the simplification from Equation (2) to (4) could be made.

2.2 Calibration of system model parameters

Two free parameters P_0 and n from the Log-Normal model of signal transmission, described in Eq. (6), need to be determined for the algorithm. These parameters depend on the transmitter hardware, receiver hardware and software, and the environment. This problem can easily be resolved by calibrating each of the receivers, if the influence of hardware and software is assumed constant and influence of the environment is neglected or assumed constant as well.

For the calibration method used in this work, a sufficient number of samples at distance d_0 have to be collected. The n parameter is chosen to be the theoretical value from the Friis transmission equation, which is 2, and the P_0 parameter is then obtained from Eq. (6) as

$$P_0 = P_r + 10n \log_{10}(d_0),$$

where P_r is the mean of sampled data and d_0 the corresponding distance. The random variable χ is presumed to have a zero mean, so for a sufficient amount of samples it will have no effect on the calibration. If the mean is not zero, it is added to P_0.

An alternative approach would be obtaining samples from different distances and then fitting a logarithmic curve in the form described above through the data with P_0 and n as free parameters. This approach was examined in the experiments described in sections 5.1 and 5.2. It has the advantage that the curve has a much smaller mean error and standard deviation from the samples and thus it may offer more precise calculation of distance from RSSI. The downside is that the n parameter is heavily dependant on the environment and even on the relative position of the receiver and transmitter from obstacles in the environment (compare the n parameters of the fitted functions in the two experiments). Because of this the first approach, which is presumed to be more robust in relation to these conditions, has been used.

3 Localization algorithm

The algorithm to locate the beacons relies on the Kalman Filter for state estimation, sensor fusion and filtration. Since the system is non-linear, the basic form of the KF would not be sufficient and a generalized variant of the KF for non-linear systems had to be chosen. Two main generalized variants are the Extended Kalman Filter and the Unscented Kalman Filter. Previous works comparing the two approaches generally come to a conclusion that the UKF offers better stability and precision for systems with strong non-linearities at the cost of higher computational intensity [20], [21], [7], [8]. The UKF can also work without determining the Jacobian of the system model and can cope for non-additive noise in the system without additional changes to the algorithm unlike the EKF. Non-additive noise is not present in the considered system model so this criterion can be ignored for the purpose of this work. Jacobian of the system can easily be calculated analytically so this criterion is irrelevant as well. To decide which algorithm to use, the simulations have been run for both of them. Since the results were almost equal for both mentioned variants of the KF, the EKF was chosen to be used further as it is less computationally demanding. For details about the simulations, see section 4.

The BLE beacons periodically transmit advertisement packets with a set period and power output. In our case, the beacons used in the experiments can be set to transmit in three states – low power with a period of $T_{TX} = 100\,\text{ms}$, medium power with $T_{TX} = 500\,\text{ms}$ and high power with $T_{TX} = 1000\,\text{ms}$. If the strength of the signal is sufficient, the packets are received by the BLE receivers, RSSI of the packets is measured and a new RSSI reading is generated. If new readings from all receivers are available, the state estimation filter is updated. Because range of the BLE beacons is limited and the area being searched can be larger than the beacon signal range, there may not always be a set of new valid measurements from all receivers. Because the estimation is updated only when a complete set of new valid measurements is ready, the time between two updates is not constant. This could potentially be a source of inaccuracies, because the non-constant time step has been neglected in the model. It might be an interesting problem for future development of this work to implement an estimation update without all new readings available.

The MAVs follow a set of points, positioned so that the whole search area is sufficiently covered. The way the trajectory points are chosen is arbitrary, the trajectory must assure that each beacon in the search area is passed at a certain maximal distance. The maximal distance should be significantly shorter than the maximal detection range of the transmitters, so that enough RSSI samples can be collected by the receivers. An example of such trajectory is the “lawn mower” approach (shown on Fig. 3), which was chosen in the simulations presented in section 4.

An estimation of the initial state must be known for the EKF. Quality of further state estimation is dependant on the initial state of the filter. Bad initial state estimation can cause the algorithm to converge to a wrong location. The initial state estimation is

required only for the beacon position, because the last measured positions of the MAVs can be used as initial estimates of the MAV position states. The beacon position initial state is estimated in $n_{initial}$ steps by a separate algorithm described in section 3.1.

3.1 Initial state estimation

The initial state estimation for the EKF is basically an average of estimates of the state $E = \begin{bmatrix} x_b, & y_b \end{bmatrix}$, representing the beacon position in two dimensions, which are calculated from intersections of M circles at each step, where M is the number of MAVs/receivers. Center of the i-th circle is defined by a position of the i-th MAV $\begin{bmatrix} x_i, & y_i \end{bmatrix}$. Its radius is equal to an estimated beacon distance from the i-th MAV d_i, calculated from the filtered RSSI signal $s_{f,i}$. The z_b state (beacon height) is not estimated. It is set to $z_b = 0$, because the beacon is presumed to be lying on the ground or in a small height above ground.

Let E be the current estimate of the beacon position, w be the current estimate weight, $s_{f,i}$ be the current filtered RSSI of the i-th MAV, and d_i be the current estimated distance of the beacon to the i-th MAV. Variables E and w are initialized to $E := \begin{bmatrix} 0, & 0 \end{bmatrix}$ and $w := 0$ before the start of the algorithm. The initial state is estimated by repeating the following algorithm $n_{initial}$ times:

1. In the first iteration, $s_{f,i}$ is set equal to the first RSSI sample $s_{f,i} := s_i$. In the subsequent iterations $s_{f,i}$ is calculated as $s_{f,i} := \frac{c_f s_{f,i} + s_i}{c_f + 1}$.

2. Distance d_i is calculated from the RSSI value $s_{f,i}$ using the Eq. (6).

3. The circles with centres $C_i = \begin{bmatrix} x_i, & y_i \end{bmatrix}$ and radii $R_i = d_i$ are defined. All intersections of each pair of the circles are calculated. If no intersection is found the algorithm ends here and no estimation update is made until the next valid set of measurements.

4. For each circle pair, there can be either one, two or no intersections. If there is zero intersections, none is chosen. If there is one intersection, it is chosen. If there are two intersection points, a sum of distances between the point and all circles is calculated for both points. The point with the smaller sum is chosen.

5. Average from the chosen points is declared to be the current point $A = \begin{bmatrix} x_A, & y_A \end{bmatrix}$ and the estimation is updated as

$$\begin{aligned} x_b &:= \frac{w x_b + x_A}{w + 1}, \\ y_b &:= \frac{w y_b + y_A}{w + 1}, \\ w &:= w + 1. \end{aligned}$$

State covariance for the EKF is calculated as $cov(x_b, x_b) = \frac{c_w}{n_{initial}}$, $cov(y_b, y_b) = \frac{c_w}{n_{initial}}$, $cov(x_b, y_b) = cov(y_b, x_b) = 0$. The constants $n_{initial}$, c_f and c_w are free parameters, which have to be tuned. The tuning is done based on experiments, simulations, and known parameters of the system model.

3.2 Extended Kalman Filter

The EKF generates state estimates $\vec{x}[k]$ and state covariance matrices $\mathbf{P}[k]$ at each estimation update. A model of the system (defined in section 2), an initial state $\vec{x}[0]$ and initial covariance matrix $\mathbf{P}[0]$ of the state vector are required. Determining $\vec{x}[0]$ and $\mathbf{P}[0]$ has been described in the previous section. At each step, the EKF also requires the previous estimated states $\vec{x}[k-1]$, previous covariance matrix $\mathbf{P}[k-1]$, current system input $\vec{u}[k]$ and current measurements $\vec{z}[k]$. An estimation step consists of state **prediction** and **update**, similarly to the classical Kalman Filter. The difference is that the EKF works with a linearization of the otherwise non-linear system model. The working point at each step is the previous state estimation. Kalman gain is calculated similarly to the standard Kalman filter and the state estimation together with its covariance matrix are updated. The EKF has two tunable parameters - the process noise and measurement noise covariance matrices $\mathbf{Q}, \mathbf{R}$. It is described in detail for example in [7] or [8].

4 Simulations

The aim of the simulation was to test the developed algorithm, its performance and its limits. Simulation of the localization algorithm was done in MATLAB. Parameters for the simulation were chosen to reflect the target practical experiments as well as possible, based on preliminary experiments (including the experiment, described in section 5.1) and the physical model. In the simulation, separate instance of the filter was used for each beacon.

An additional target was determining which variant of the KF is better suited for this application - the UKF or the EKF. This was done by running one instance of the UKF and one instance of the EKF for each beacon being localized, and then comparing the results. The simulation was done with $N_{beacons} = 10000$ randomly generated beacon positions and $M = 3$ MAVs. Results of the simulation are described in Section 4.2.

4.1 Simulation parameters

The system has been modelled according to the model described in section 2, adopted to two dimensions (all states, corresponding to the z coordinate have been trimmed).

The RSSI readings for the algorithm have been generated based on the Equation 6. The mean of the random variable χ (representing signal noise) has been assumed to be non–zero when generating the readings, but assumed equal to zero in the model used by the algorithm. Unknown non–zero mean noise can be caused by non–ideal conditions of signal propagation, imprecisely determined parameters $P_{0,i}$ and possibly other causes. Additionally, a maximal beacon signal range r_{max} has been introduced. This was based on the assumption, that when the SNR value drops under a certain threshold, the transmitted packet is lost and RSSI cannot be measured by the receiver. This assumption was supported by the preliminary experiments. When the beacon is further than r_{max} from the receiving MAV in the simulation, no reading is generated and thus the KF estimation step is not performed.

The following parameters have been used for the model:

$$\mathbf{Q} = \begin{pmatrix} 0.01 \cdot \mathbf{I}_{6\times6} & \mathbf{0}_{6\times2} \\ \mathbf{0}_{2\times6} & \mathbf{0}_{2\times2} \end{pmatrix},$$

$$\mathbf{R} = \begin{pmatrix} 0.01 \cdot \mathbf{I}_{6\times6} & \mathbf{0}_{6\times3} \\ \mathbf{0}_{3\times6} & 5 \cdot \mathbf{I}_{3\times3} \end{pmatrix},$$

$$
\begin{aligned}
P_{0,i} &= -40.23\,\text{dBm}, \\
n_i &= 2, \\
r_{max} &= 4\,\text{m}, \\
\mu_\chi &= \pm 2\,\text{dBm}, \\
\sigma_\chi^2 &= 5\,\text{dBm}.
\end{aligned}
$$

The algorithm can be more sensitive to a positive change of the parameter P_0 than a negative change or vice versa, because the system is non–linear. This means that if the parameter μ_χ was set equal to 2 dB, the simulation could give different results than for $\mu_\chi = -2\,\text{dB}$. To eliminate this influence the μ_χ parameter has been drawn from a binary random distribution for each transmitter/receiver combination, with the following probability distribution:

μ_χ	Probability
$-2\,\text{dBm}$	0.5
$2\,\text{dBm}$	0.5

Table 3: Probability distribution of the RSSI noise mean

Some of the other system parameters are not precisely determined in a practical application. This has been included in the simulation and the model parameters (specifically the random noise covariance matrices $\mathbf{Q}_{KF}$ and $\mathbf{R}_{KF}$), presented to the Kalman Filter, are different from the parameters, used to generate the measurements. The covariances were assumed to be overestimated:

$$
\mathbf{Q}_{KF} = \begin{pmatrix} 0.05 \cdot \mathbf{I}_{6\times 6} & \mathbf{0}_{6\times 2} \\ \mathbf{0}_{2\times 6} & \mathbf{0}_{2\times 2} \end{pmatrix},
$$

$$
\mathbf{R}_{KF} = \begin{pmatrix} 0.05 \cdot \mathbf{I}_{6\times 6} & \mathbf{0}_{6\times 3} \\ \mathbf{0}_{3\times 6} & 9 \cdot \mathbf{I}_{3\times 3} \end{pmatrix}.
$$

The UKF also depends on three parameters determining the weighing and generation of sigma points. These are α, β and κ. They were chosen to be the default values for Gaussian distribution of the process and measurement noise:

$$
\begin{aligned}
\alpha &= 10^{-3}, \\
\beta &= 2, \\
\kappa &= 0.
\end{aligned}
$$

A rectangle with dimensions $a_{rec} \times b_{rec}$ defines the search area, where 10 beacons are randomly placed. The rectangle size was chosen to reflect the target practical application. The MAVs follow a set of trajectory points in a formation. The points are generated in

a simple "lawn mower" pattern to cover the area evenly (see Figure 3). This way the formation center does not fly further than 2 m around any beacon, placed in the area. The 2 m detection radius was chosen based on preliminary experiments. It should ensure that all beacons are in detection range for a sufficient amount of time to localize them accurately. MAV dynamics are not simulated. It is assumed that they move between the trajectory points with a constant speed v for simplicity. Duration of simulation t_{end} is the time it takes the MAV formation to reach the end of its trajectory. Parameter f_{RSSI} is the frequency of receiving new signal readings. The values of these parameters are

$$\begin{aligned} a_{rec} &= 4\,\mathrm{m}, \\ b_{rec} &= 8\,\mathrm{m}, \\ v &= 0.2\,\mathrm{m\,s^{-1}}, \\ t_{end} &= 320\,\mathrm{s}, \\ f_{RSSI} &= 10\,\mathrm{Hz}. \end{aligned}$$

Following values were experimentally chosen for the initial state estimation parameters:

$$\begin{aligned} n_{initial} &= 30, \\ c_f &= 3, \\ c_w &= 500. \end{aligned}$$

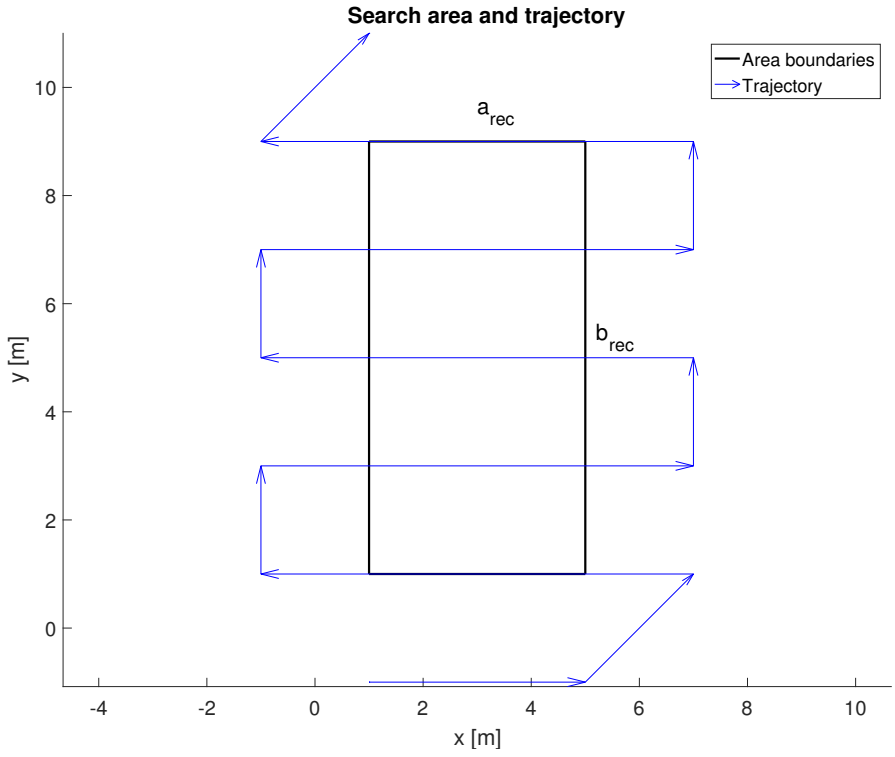

Figure 3: Trajectory of the MAV formation over the defined search area

4.2 Results

An error e is defined as a euclidean distance between the true position $\begin{bmatrix}\hat{x}_b, & \hat{y}_b\end{bmatrix}^T$ and the resulting position estimate $\begin{bmatrix}x_b, & y_b\end{bmatrix}^T$ for each beacon:

$$e = \sqrt{(x_b - \hat{x}_b)^2 + (y_b - \hat{y}_b)^2}.$$

The average error distances from all 10000 beacons for the UKF and EKF variants of the algorithm were

$$\overline{e}_{UKF} = 0.243\,\mathrm{m},$$
$$\overline{e}_{EKF} = 0.234\,\mathrm{m}.$$

Also the distributions of the distance errors were very similar for both the UKF and the EKF (see Figure 4). The total calculation time for the 10000 beacons were

$$t_{UKF} = 1658\,\mathrm{s},$$
$$t_{EKF} = 868\,\mathrm{s}.$$

For this type of system the difference in precision between the UKF and the EKF is relatively small (less than 1 cm on average). Big difference is in the computational time, the EKF is almost 91% faster. The EKF will be used in the rest of this work because of the speed advantage. The average CPU time of one algorithm step when using the EKF is

$$t_{step} = \frac{t_{EKF}}{N_{beacons} \cdot t_{end} \cdot f_{RSSI}} = \frac{868\,\mathrm{s}}{10000 \cdot 320\,\mathrm{s} \cdot 10\,\mathrm{Hz}} \doteq 27\,\mu\mathrm{s}.$$

This suggests that the algorithm might be sufficiently fast for realtime operation as well, because the maximal desired time between updates is $\frac{1}{f_{RSSI}} = 100\,\mathrm{ms}$. But it must be taken into account that the simulation was run on a desktop computer with usually more computational power than the onboard computer.

The simulation results were proven to be reasonable when compared to results of the practical experiments (described in Sections 5.3, 5.4 and 5.5), although a bit optimistic. This was expected as the simulation was simplified and did not cover all possible real world conditions and imperfections (for example signal reflections from obstacles, non–uniformity of transmitting or receiving antennae, time drift of onboard computers on the MAVs, etc.).

The conclusion is that this approach is viable, sufficiently precise and stable, although the maximal error is quite large. This might be caused by a bad initial state of the KF. Making the initial state estimating algorithm more robust is a topic for future work on this project.

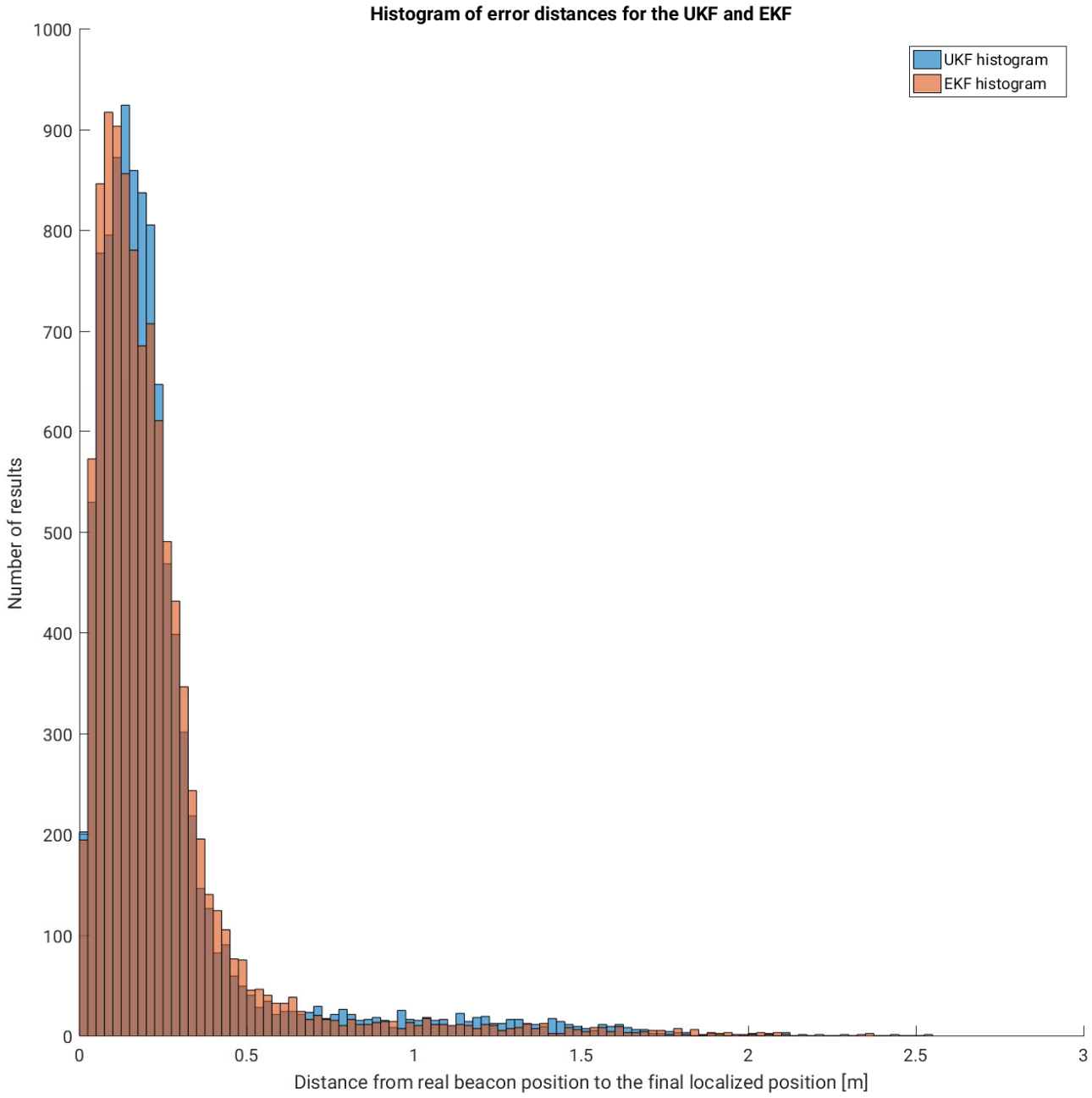

Figure 4: Histogram of simulation result - distances between true and found positions

5 Practical experiments

Two experiments (described in sections 5.1 and 5.2) were conducted to determine viability of the BLE technology for this application. The experiments consisted of measuring the RSSI over receiver/transmitter distance characteristic of a BLE beacon. In each of these experiments, 100 samples of RSSI were measured at several distances from the beacon.

Another two experiments (described in sections 5.3 and 5.4) were aimed at determining stability of the localization algorithm under real world conditions. In these experiments, one BLE beacon has been placed in an area and one MAV carrying a BLE receiver flew through a preprogrammed trajectory in the area, and logged its position in time together with RSSI measurements. The logged data were processed offline after the experiments.

The final experiment (described in section 5.5) has been conducted with three MAVs hovering in a static position, two static beacons and one dynamic beacon, placed on a ground robot. This was the closest to the desired system setup, except that the MAVs were not moving. The dynamic beacon together with the dynamic obstacle, introduced into the system by the ground robot moving through the area, presented a new challenge.

5.1 Outdoor RSSI measurement experiment

The first experiment was aimed at determining the general usability of the bluetooth technology and the possibility to improve the precision of range calculation through calibration of the model parameters. It has been conducted outdoors in a paved backyard. A laptop (Samsung NF310) with a USB BLE adapter (Trust 18187-03) and a BLE beacon (EM Electronics EMBC01) were positioned approximately 3 cm above ground at distance d. RSSI values were measured at nine different distances and logged to data files. The data were then compared to the theoretical function (according to Equation (6)). The unknown parameter n was chosen to be 2, according to the Friis function (Eq. 5), and $P_0 = -82.64\,\mathrm{dB}$ was obtained as explained in Section 2.2.

Let e_i be an error of the i-th measured sample and the corresponding theoretical value. This random variable has a mean $\mu = 2.08\,\mathrm{dBm}$ and a standard deviation $\sigma = 3.87\,\mathrm{dBm}$, which were obtained as

$$
\begin{aligned}
e_i &= s_i - s_{theoretical,i}, \\
\mu &= \frac{1}{N}\sum_{i=1}^{N}\left(e_i\right), \\
\sigma &= \sqrt{\frac{1}{N-1}\sum_{i=1}^{N}\left(\mu - e_i\right)^2},
\end{aligned}
$$

where $N = 100$ is the number of samples, s_i is the i-th sample and $s_{theoretical,i}$ is the value of the Log-Normal function (5) for the same distance as sample s_i.

The above mentioned result can be improved by adjusting the Log-Normal function. The measured samples were fitted with a logarithmic function using the least squares method. The resulting error had a standard deviation 3.77 dBm and a mean of 0.002 dBm. This fits the system model (as described in Section 2), where zero–mean random noise has been assumed, better than if using the n parameter from the Friis formula and calculating only P_0. Parameters of the fitted function were $n = 2.303$ and $P_0 = -80.97$ dBm.

A plot of the measured samples with the theoretical and fitted curves can be seen in Figure 5. Note that there are no data points further than 1.8 m. No RSSI readings have been captured further because the signal was too weak.

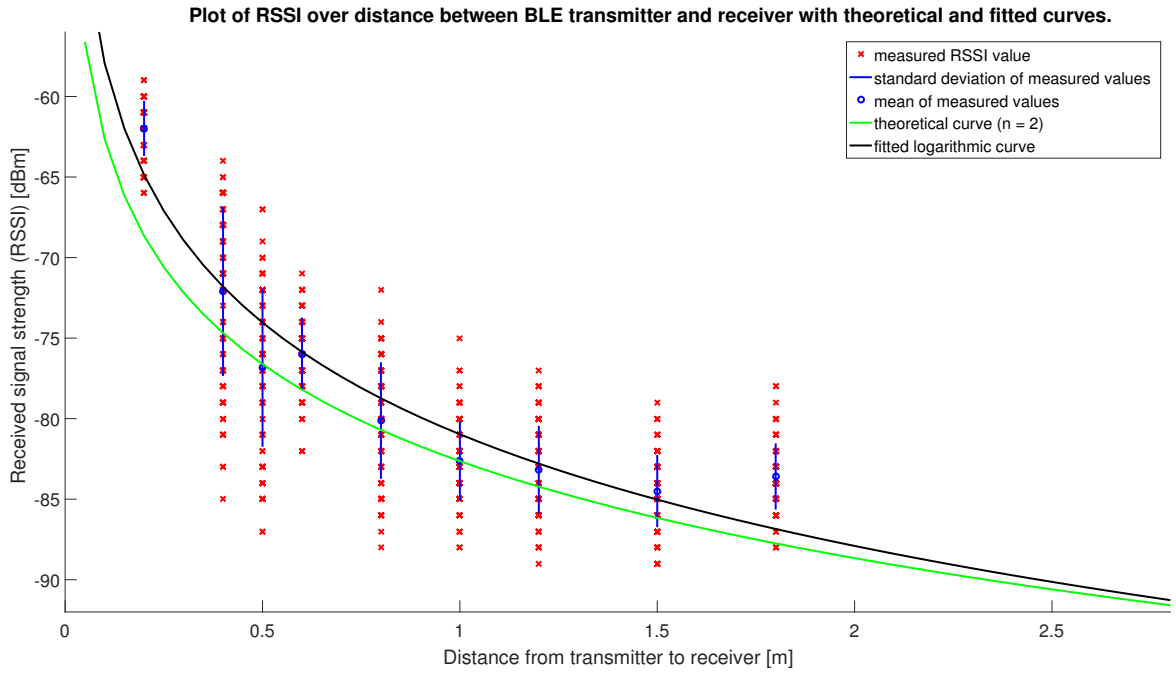

Figure 5: Plot of results from the outdoor RSSI measurements

5.1.1 Conclusion

The non-zero mean of the noise might introduce error when localizing the beacons, but according to the simulation, presented in section 4, the precision should still be sufficient. Another problem might be the short signal range. This was caused most probably by the beacon lying almost on the ground, because a significant amount of the transmitted power was absorbed. In the following experiments, the beacon has been placed on a plastic stand approximately 8 cm above ground, to prevent this problem. Significant increase in signal

range has been observed in the subsequent experiments, which is probably thanks to this. Although there is a clear relation between the transmitter/receiver distance and RSSI, the signal noise is not negligible. This supports the decision to use the KF in the localization algorithm, which also filters the noise out of the signal alongside the state estimation, as opposed to other localization methods, which mostly require a separate filter (these methods are referenced in section 1.1). Generally, this experiment has shown that the bluetooth technology should be usable for purposes of this thesis.

5.2 Indoor RSSI measurement experiment

The second experiment was aimed at determining the usability of the hardware in indoor areas and confirming or disproving the assumption that the signal range will be much longer when the receiver and transmitter are in a higher position. It has been conducted indoors in a mostly empty hallway. The MAV onboard PC (Nvidia TK1) with a USB BLE adapter (Trust 18187-03) was positioned at a height of 0.65 m and the BLE beacon (EMBC01) at a height of 8 cm above ground. RSSI values were measured and processed similarly to the first experiment (Section 5.1).

The parameters of the Log-Normal function have been determined in the same way as in the previous experiment. First, by choosing n to equal the theoretical value from the Friis function and calculating only P_0. These parameters were $n = 2$ and $P_0 = 185.35\,\text{dBm}$ and the corresponding error has a mean of $-1.09\,\text{dBm}$ and a standard deviation $5.40\,\text{dBm}$. Then a logarithmic function has been fitted through the data. The error of sampled data and the fitted function has a mean of $-0.05\,\text{dBm}$ and a standard deviation $4.88\,\text{dBm}$. Parameters of the fitted function were $n = 1.091$ and $P_0 = 182.00\,\text{dBm}$. A plot of the measured samples with the theoretical and fitted curves can be seen in Figure 6.

5.2.1 Conclusion

The RSSI over distance characteristic is significantly further from the idealized theoretical values of the Friis function in the experiment in indoor environment than in the outdoor experiment. The RSSI measurements do not even show a monotone behaviour, relatively to the distance, as would be expected according to the theoretical function. This anomaly and the larger error are assumed to be due to reflections of the signal from walls, furniture and other obstacles. As a consequence, the algorithm might be unusable in such environment. The RSSI offset (P_0 parameter) is much more different from the outdoor experiment (described section 5.1) than what could be caused by the different environment (the difference is $267.98\,\text{dBm}$ and maximal span of the RSSI values is less than $35\,\text{dBm}$ in both experiments). Since the hardware and software was the same except the computer platform and corresponding OS, a significant part of the large P_0 difference is presumed

to be caused by a different implementation of the BLE driver on the two platforms. This shows the importance of calibrating the P_0 parameter for each hardware setup separately.

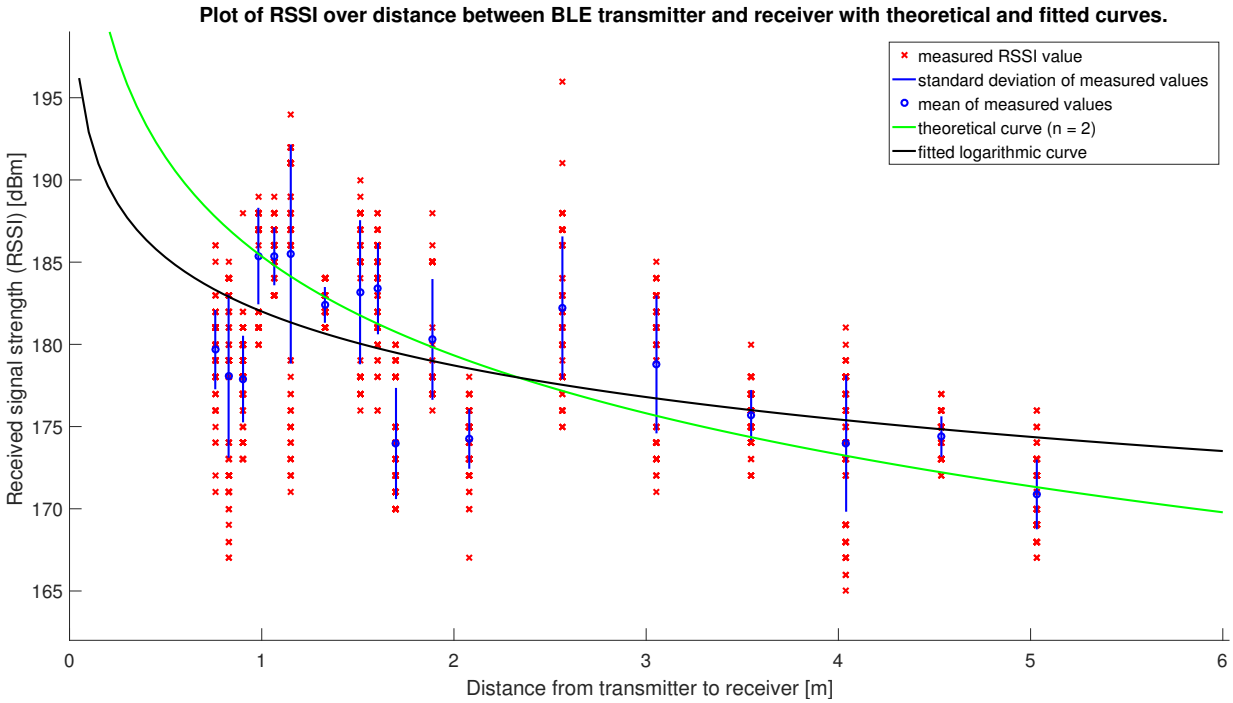

Figure 6: Plot of results from the indoor RSSI measurements

5.3 Experiment with one MAV following a square trajectory

The third experiment was aimed at determining stability and performance of the localization algorithm under real world conditions. It has been conducted in indoor environment with one MAV flying through a square trajectory setpoint around the BLE beacon (EMBC01). The MAV carried a USB BLE adapter (Trust 18187-03), connected to onboard PC (Nvidia Tegra TK1 development kit). MAV speed was set to $0.2\,\mathrm{m\,s^{-1}}$. Setpoint following and data logging was provided by the onboard controller. Signal strength has been measured with a frequency of 10 Hz and logged together with the current position, obtained from the onboard sensors. This data has then been processed after the experiment in MATLAB.

The MAV repeatedly followed a square trajectory 1 m above ground with a size of $4\,\mathrm{m} \times 4\,\mathrm{m}$ and the beacon was put in the middle of this square, as shown in Figure 8. The system model described in section 2, adapted for one MAV, has been used for processing the data. Following parameter values were used in the model:

$$\mathbf{Q} = \begin{pmatrix} 10^{-4} \cdot \mathbf{I}_{3\times3} & \mathbf{0}_{3\times3} \\ \mathbf{0}_{3\times3} & 5 \cdot 10^{-7} \cdot \mathbf{I}_{3\times3} \end{pmatrix},$$

$$\mathbf{R} = \begin{pmatrix} 0.05 \cdot \mathbf{I}_{3\times3} & \mathbf{0}_{3\times1} \\ \mathbf{0}_{1\times3} & 8 \cdot \mathbf{I}_{1\times1} \end{pmatrix},$$

$$P_{0,1} = 187\,\text{dBm},$$
$$n_1 = 2.$$

The parameters were tuned based on data from the other experiments and simulations. The initial state and covariance matrix have been chosen as

$$\begin{aligned} \vec{x}[0] &= \begin{bmatrix} x_1[0], & y_1[0], & z_1[0], & 3.5, & 3.5, & 0.08 \end{bmatrix}^T, \\ &= \begin{bmatrix} 0, & 2, & 1, & 3.5, & 3.5, & 0.08 \end{bmatrix}^T, \end{aligned}$$

$$\mathbf{P}[0] = \begin{pmatrix} 0.05 \cdot \mathbf{I}_{3\times3} & \mathbf{0}_{3\times3} \\ \mathbf{0}_{3\times3} & 50 \cdot \mathbf{I}_{3\times3} \end{pmatrix},$$

where the initial MAV position was the actual MAV position at the timestep $k = 0$, as measured by the onboard sensors. The initial beacon position cannot be determined by the algorithm as described in Section 3.1, because one signal reading is not enough for it. It had to be chosen randomly and it was chosen to be different from the true beacon position. If the initial state estimation algorithm could be used, the resulting estimation would be most likely closer to the true position than the randomly chosen position. This speculation is supported by the simulation and further experiments. The initial covariance of the beacon position suffers a similar problem as it cannot be determined by the algorithm. It was chosen relatively large so that the initial position has a low weight since it was chosen randomly.

Data were evaluated from a 334 s long flight. The resulting MAV trajectory can be seen in Figure 8. For evaluation of the algorithm performance, the beacon has been positioned at the origin of the coordinate system. The true beacon position is then

$$\begin{bmatrix} \hat{x}_b, & \hat{y}_b, & \hat{z}_b \end{bmatrix}^T = \begin{bmatrix} 0, & 0, & 0 \end{bmatrix}^T$$

Since the true beacon position is known, it can be used to determine a localization error. The localization error can be defined as a euclidean distance between the true and found position as

$$e = \sqrt{(x_b - \hat{x}_b)^2 + (y_b - \hat{y}_b)^2 + (z_b - \hat{z}_b)^2}.$$

Figure 7 is a plot of the resulting position error. The final beacon position found from the measured RSSI and position data is

$$\vec{p}_b\,[k_{end}] = \begin{bmatrix} -0.68, & -0.05, & 1.00 \end{bmatrix}^T,$$

i.e. the final error is 1.14 m.

5.3.1 Conclusion

The error of the estimated beacon position does not converge to zero, but rather oscillates between two values. This can clearly be seen in the position error graph. This phenomenon can be correlated to a significant raise in RSSI in an area around the bottom left corner of the trajectory setpoint square. In Figures 7 and 9, the marks denote time when the error has started increasing and the corresponding MAV positions. The cause of this anomalous signal strength raise has been speculated to be a thick concrete column near to that area, which may have been a strong source of signal reflections and thus signal interference. This conveniently highlights the downsides and limits of the BLE technology for this approach in indoor areas as the RSSI is very sensitive to obstacles and reflections.

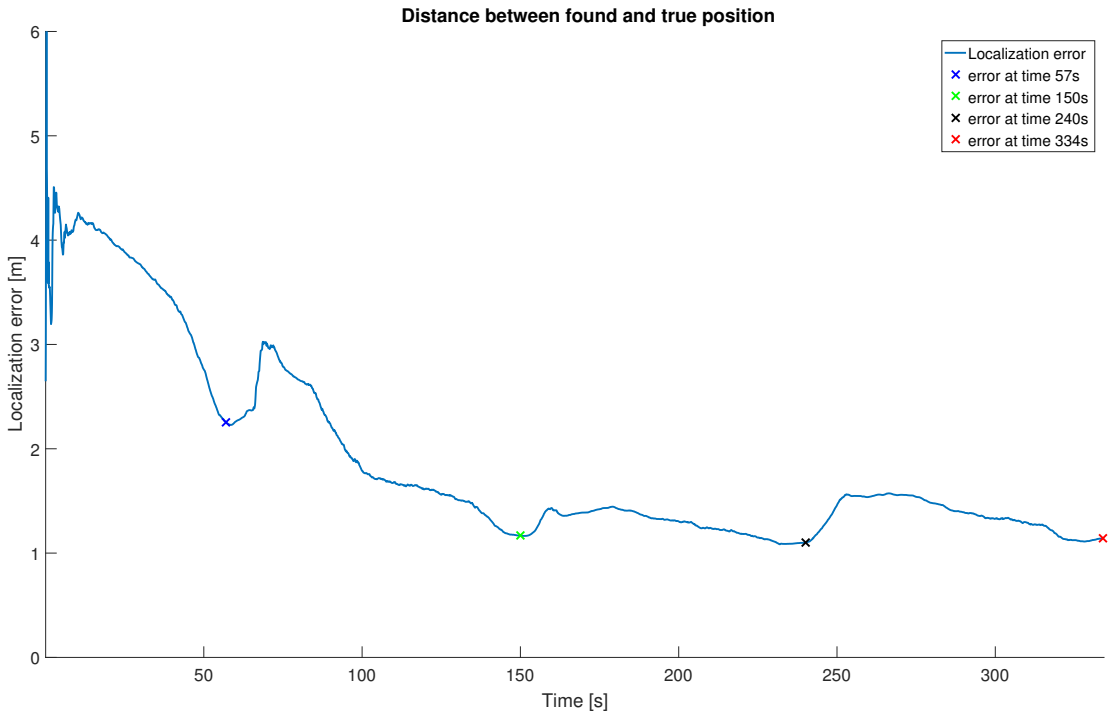

Figure 7: Distance between the true and found beacon position over time in this experiment

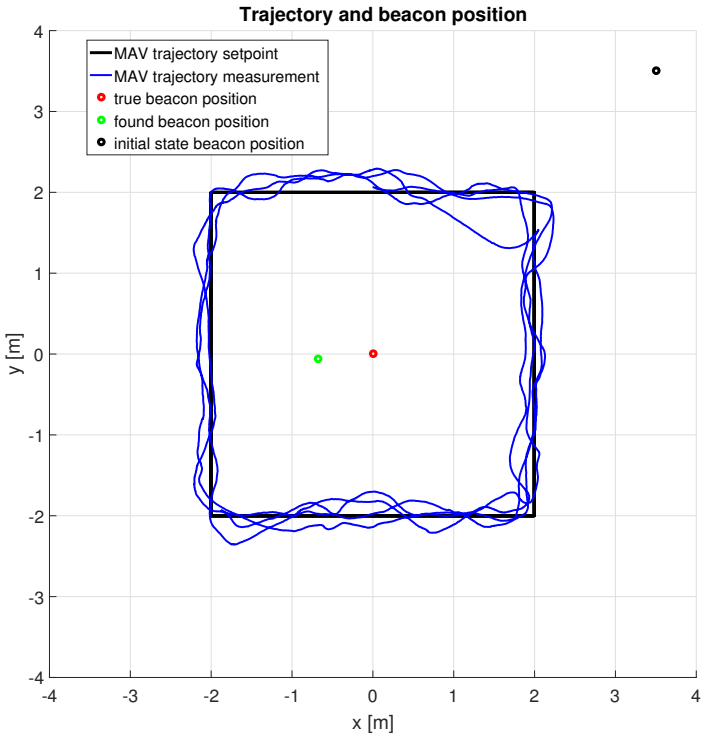

Figure 8: Trajectory of the MAV in this experiment

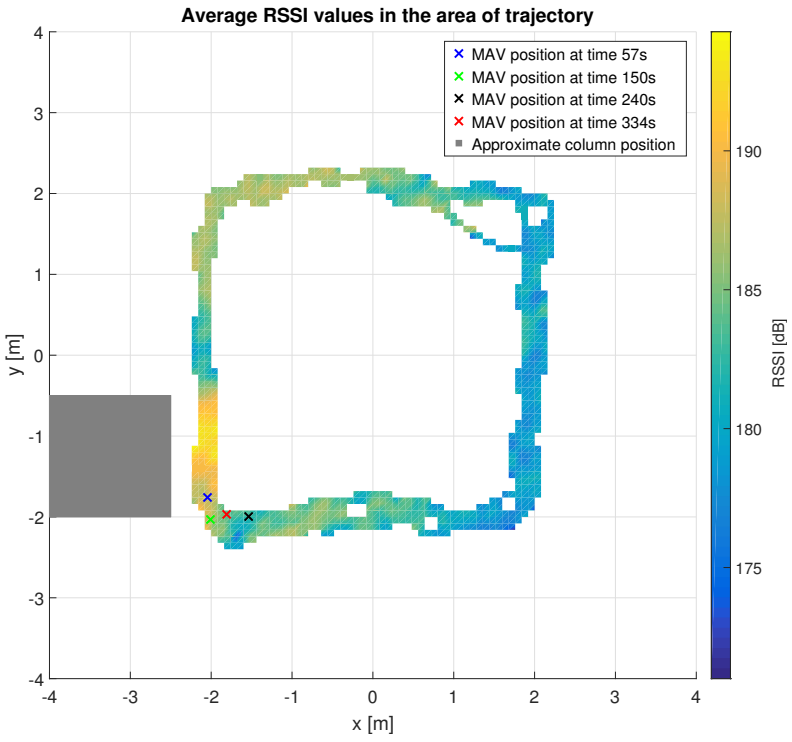

Figure 9: Average measured RSSI values in different areas of the trajectory

5.4 Experiment with one MAV following a line trajectory

In this experiment, the same hardware configuration as in the experiment 5.3 has been used, but the trajectory of the MAV was a 6 m long line segment. The beacon remained in the origin of the coordinate system. The MAV speed, data logging frequency and all other parameters remained the same as in the previous experiment. The algorithm and the position error were also defined in the same way. The experiment took place in the same room. Data were evaluated from 458 s long flight. Initial state for the EKF was

$$\begin{aligned}\vec{x}[0] &= \begin{bmatrix} x_1[0], & y_1[0], & z_1[0], & 0, & 2, & 0.08 \end{bmatrix}^T \\ &= \begin{bmatrix} -2.7, & -0.1, & 1, & 0, & 2, & 0.08 \end{bmatrix}^T .\end{aligned}$$

The specific location for the initial beacon position has been randomly chosen for the same reasons as in the previous experiment. The initial covariance matrix for the EKF was the same as in the previous experiment.

The resulting found beacon position is

$$\vec{p}_b\,[k_{end}] = \begin{bmatrix} -0.23, & -0.37, & 0.29 \end{bmatrix}^T ,$$

and the corresponding error is 0.48 m. Plots of the desired trajectory, real trajectory and the beacon true and found positions can be seen in Figure 10. Plot of the distance error over time can be seen in Figure 11.

5.4.1 Conclusion

As can be seen from the position error plot in Figure 11, the found position is nearly stable after three minutes. The resulting position does not oscillate as much and is generally more precise in comparison to the previous experiment, which can be explained by a lack of a signal disturbance as in the previous experiment (the MAV did not fly near the column in this experiment).

It may be speculated that with absence of the signal disturbance the previous experiment would be more precise, because the square trajectory is more suitable for the algorithm, as data are provided from more diverse locations than if following the line trajectory, which may positively affect the efficiency of the algorithm.

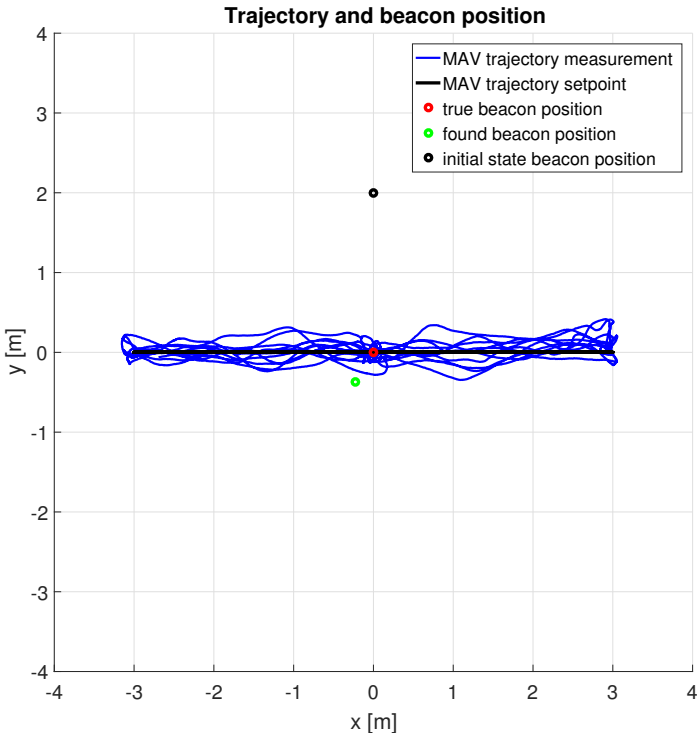

Figure 10: Trajectory of the MAV in this experiment

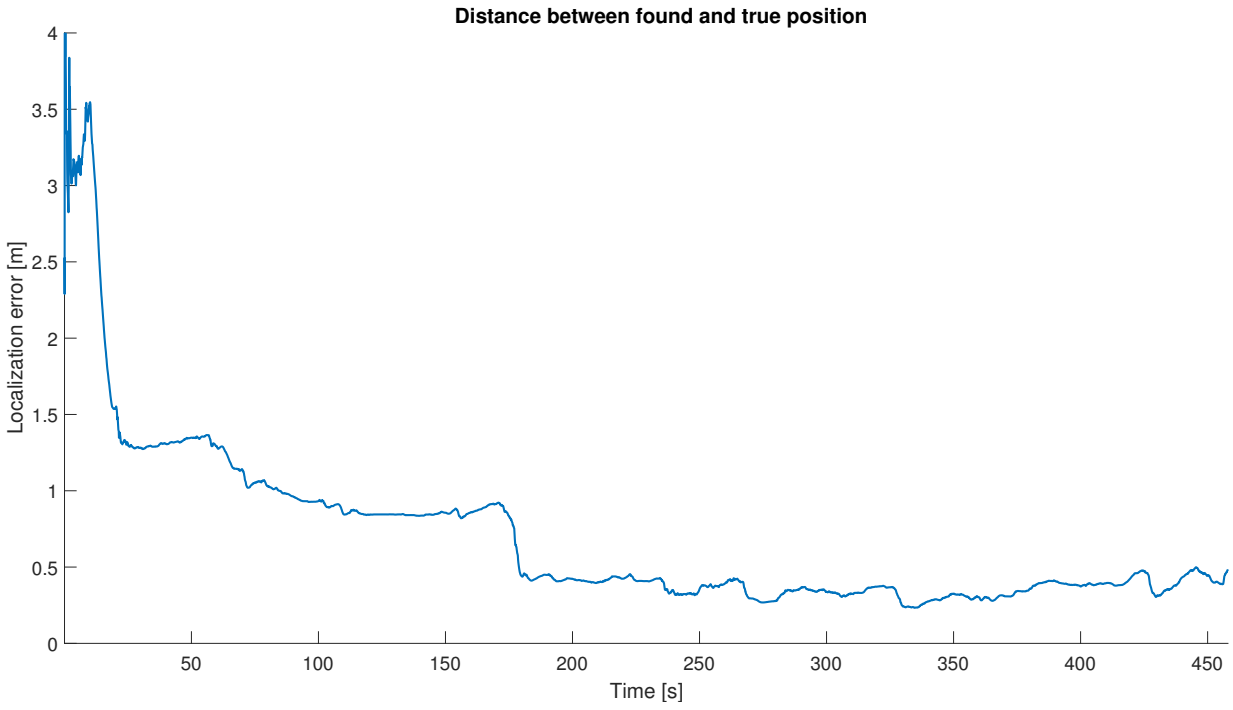

Figure 11: Distance between the true and found beacon position in this experiment

5.5 Experiment with a formation of 3 MAVs, localizing static and dynamic beacons

This experiment has been set up indoors and according to the target system setup as described in the section 1.2. The MAVs were holding their defined positions, 1 m in above ground. Three beacons have been localized. Two static beacons were placed on small ground pedestals 8 cm above ground. One beacon was dynamic, carried by an unmanned ground vehicle (UGV) 0.65 m above ground. The UGV carried the beacon through the area at speed $v = 0.2\,\mathrm{m\,s^{-1}}$ along a 6 m long straight line, parallel with the x-axis of the coordinate system. Each MAV carried one BLE receiver and logged the RSSI values together with their current positions relative to the starting points, which were acquired from the onboard odometry. The beacons were set to transmit the advertisement packets with a stronger power and a frequency of $f_{RSSI} = 5\,\mathrm{Hz}$, because the signal was too weak with the previously used setting of 10 Hz advertising with lower power. Photos of the experiment at three different times can be seen in Figure 12, setup of the experiment can be seen on the photo in Figure 13 and a photo of the UGV and one of the MAVs can be seen in Figure 14. The positions and the dynamic beacon trajectory are depicted together with the corresponding values in Figure 15.

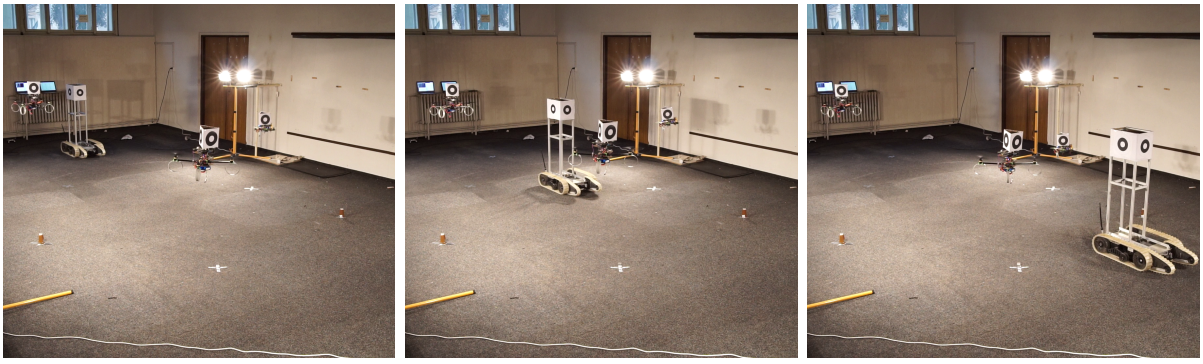

(a) Experiment, time $t = 20\,\mathrm{s}$ (b) Experiment, time $t = 35\,\mathrm{s}$ (c) Experiment, time $t = 50\,\mathrm{s}$

Figure 12: Three photos, demonstrating movement of the UGV through the experiment. The UGV has started moving at time $t = 20\,\mathrm{s}$ and stopped at time $t = 50\,\mathrm{s}$.

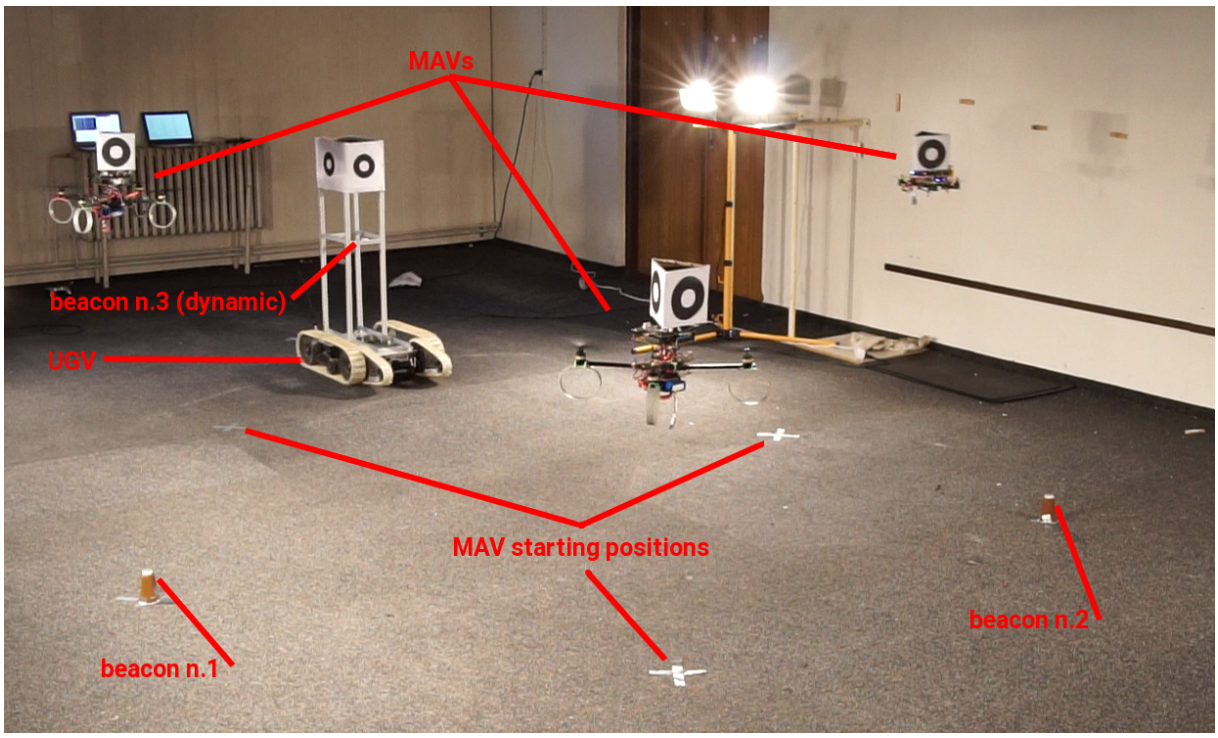

Figure 13: A photo, showing the experiment setup

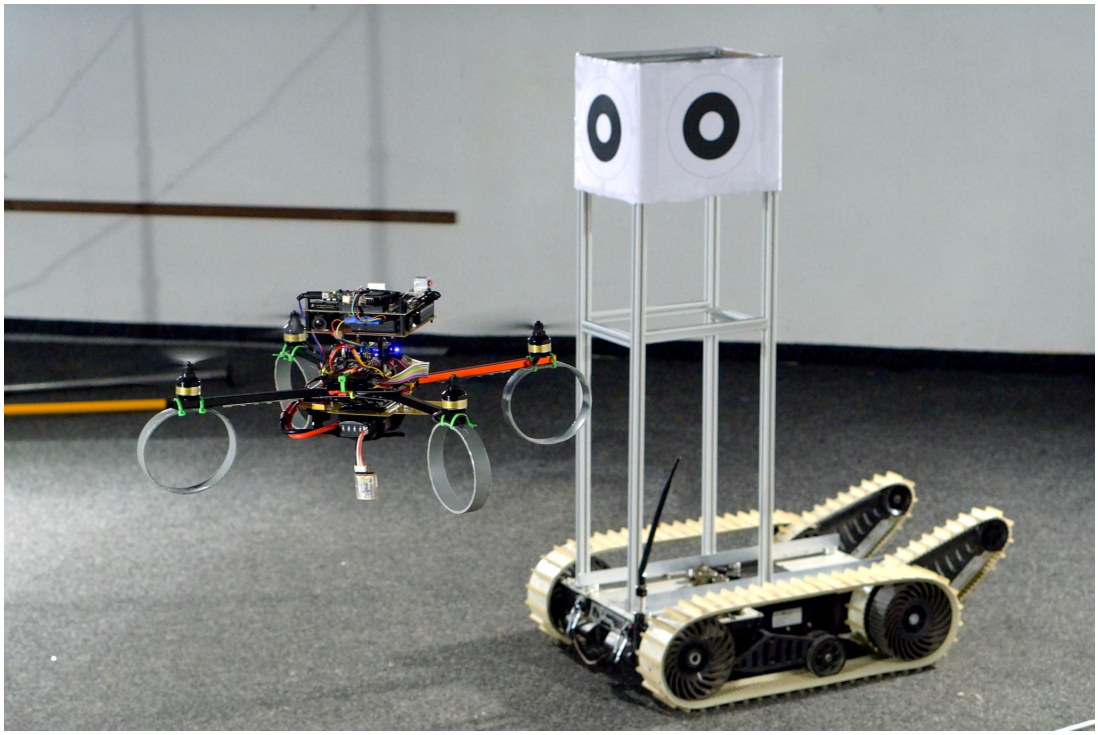

Figure 14: A photo of one of the MAVs (left) and the UGV (right)

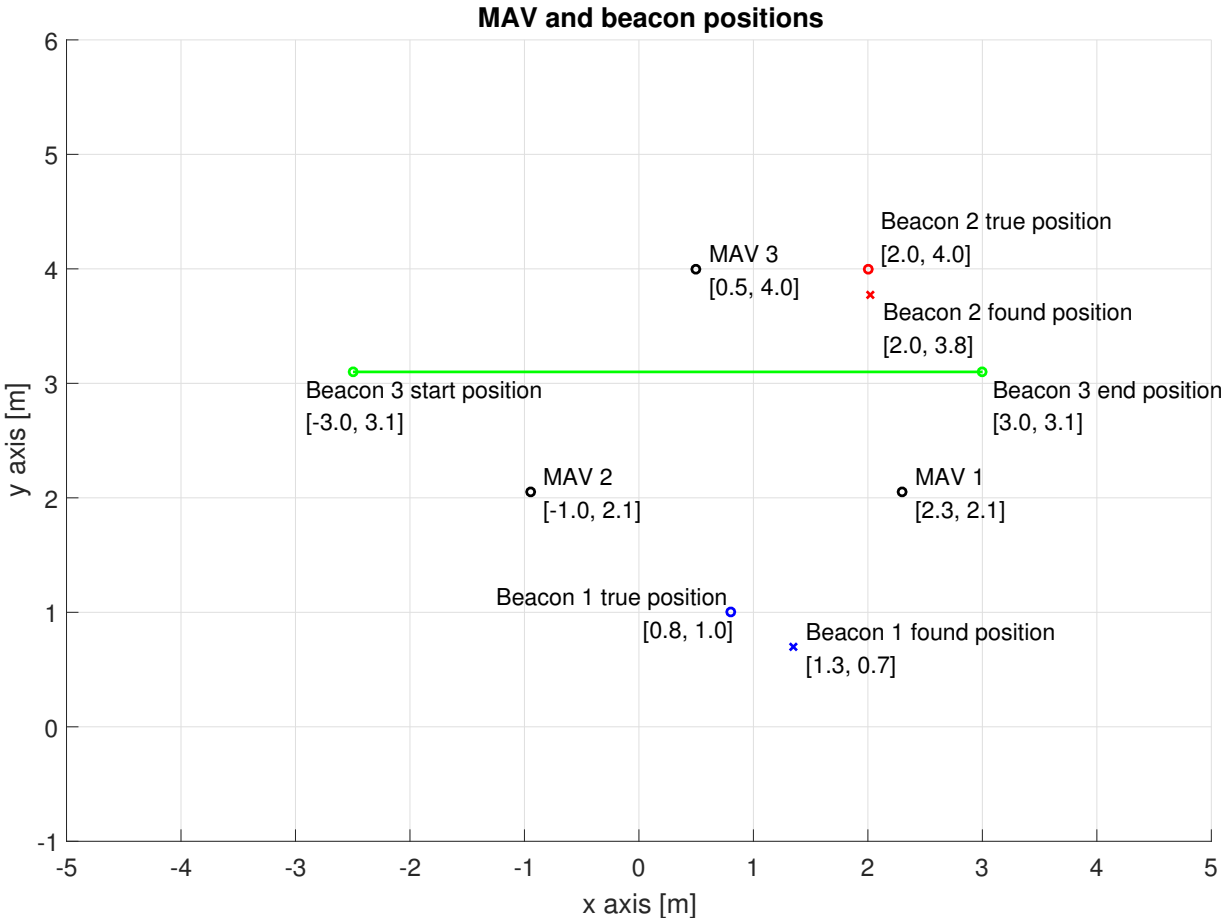

Figure 15: Positions of beacons and initial positions of MAVs in this experiment

The system has been modelled as described in section 2. Parameters and variables described in Tables 1 and 2 are used in this section with the modification that the last lower index of each parameter/variable determines to which beacon (labeled 1, 2 and 3) it corresponds. For example a set of calibrated parameters $P_{0,i,j}, n_{i,j}$ correspond to each beacon and MAV combination, where i is the number of the MAV and j is the number of the beacon. Beacon n. 3 is the dynamic beacon and a slightly modified process noise covariance matrix $\mathbf{Q}_3$ has been used for this one to account for its changing position. The x and y odometry data had to be summed with the starting points $\left[x_{i,j}[0],\ \ y_{i,j}[0]\right]$ of the MAVs because the optical odometry sensors on the MAVs are only relative (to the starting position). The $x_{i,j}[0]$ and $y_{i,j}[0]$ values are listed below. The logged z data is already measured absolutely from ground using an ultrasonic rangefinder, so it didn't need to be adjusted. Parameter values are:

$$\mathbf{Q}_1 = \mathbf{Q}_2 = \begin{pmatrix} 10^{-4} \cdot \mathbf{I}_{9\times 9} & \mathbf{0}_{9\times 3} \\ \mathbf{0}_{3\times 9} & 5 \cdot 10^{-7} \cdot \mathbf{I}_{3\times 3} \end{pmatrix},$$

$$\mathbf{Q}_3 = \begin{pmatrix} 10^{-4} \cdot \mathbf{I}_{9\times9} & \mathbf{0}_{9\times3} \\ \mathbf{0}_{3\times9} & 0.01 \cdot \mathbf{I}_{3\times3} \end{pmatrix},$$

$$\mathbf{R}_1 = \mathbf{R}_2 = \mathbf{R}_3 = \begin{pmatrix} 0.05 \cdot \mathbf{I}_{9\times9} & \mathbf{0}_{9\times3} \\ \mathbf{0}_{3\times9} & 8 \cdot \mathbf{I}_{3\times3} \end{pmatrix},$$

$$\begin{aligned} P_{0,1,1} &= 196\,\text{dB}, & P_{0,1,2} &= 195\,\text{dB}, & P_{0,1,3} &= 188\,\text{dB}, \\ P_{0,2,1} &= 196\,\text{dB}, & P_{0,2,2} &= 195\,\text{dB}, & P_{0,2,3} &= 188\,\text{dB}, \\ P_{0,3,1} &= 194\,\text{dB}, & P_{0,3,2} &= 193\,\text{dB}, & P_{0,3,3} &= 184\,\text{dB}, \\ & & n_{i,j} &= 2, & & \end{aligned}$$

$$n_{initial} = 10, \qquad c_f = 3, \qquad c_w = 15,$$

$$\vec{x}_i[0] = \begin{bmatrix} x_{1,j}[0], & y_{1,j}[0], & z_{1,j}[0], & \ldots, & x_{3,j}[0], & y_{3,j}[0], & z_{3,j}[0], & x_{b,j}[0], & y_{b,j}[0], & z_{b,j}[0] \end{bmatrix},$$

$$\begin{aligned} x_{1,j}[0] &= 2.3\,\text{m}, & x_{2,j}[0] &= -1\,\text{m}, & x_{3,j}[0] &= 0.5\,\text{m}, \\ y_{1,j}[0] &= 2.1\,\text{m}, & y_{2,j}[0] &= 2.1\,\text{m}, & y_{3,j}[0] &= 4\,\text{m}. \end{aligned}$$

The covariance matrices $\mathbf{Q}_j$ and $\mathbf{R}_j$ were chosen to be the same as in previous experiments, where these values proved to be reasonable. The parameters $P_{0,i,j}$ were calibrated as explained in section 2.2 and parameters $n_{i,j}$ were chosen equal to the theoretical value $n_{i,j} = 2$, according to the Friis formula in Eq. (5). Starting points $\begin{bmatrix} x_{i,j}, & y_{i,j} \end{bmatrix}$ were measured before the experiment. The algorithm, described in section 3.1 has been used in this experiment to estimate the initial states and initial covariance for the KF. Three constants $n_{initial}$, c_f and c_w had to be tuned for this algorithm. The beacon positions have been measured in order to evaluate the accuracy as

$$\hat{\vec{p}}_{b,1} = \begin{bmatrix} 0.8, & 1 \end{bmatrix}, \quad \hat{\vec{p}}_{b,2} = \begin{bmatrix} 0.8, & 1 \end{bmatrix}, \quad \hat{\vec{p}}_{b,3}[0] = \begin{bmatrix} -3, & 3.1 \end{bmatrix}, \quad \hat{\vec{p}}_{b,3}[k_{end}] = \begin{bmatrix} 3, & 3.1 \end{bmatrix}.$$

Note that the position of the third beacon is a function of the time step k, because the beacon was moving.

Data were evaluated from a 59 s long flight. The found beacon positions and the corresponding position errors were

$$\begin{aligned} \vec{p}_{b,1}[k_{end}] &= \begin{bmatrix} 1.35, & 0.70, & -0.38 \end{bmatrix}, & e_1 &= 0.78\,\text{m}, \\ \vec{p}_{b,2}[k_{end}] &= \begin{bmatrix} 2.02, & 3.77, & -0.07 \end{bmatrix}, & e_2 &= 0.28\,\text{m}, \\ \vec{p}_{b,3}[k_{end}] &= \begin{bmatrix} 1.84, & 2.93, & 0.33 \end{bmatrix}, & e_3 &= 1.22\,\text{m}. \end{aligned}$$

A graph of the distance error over time for the three beacons can be seen in Figure 16.

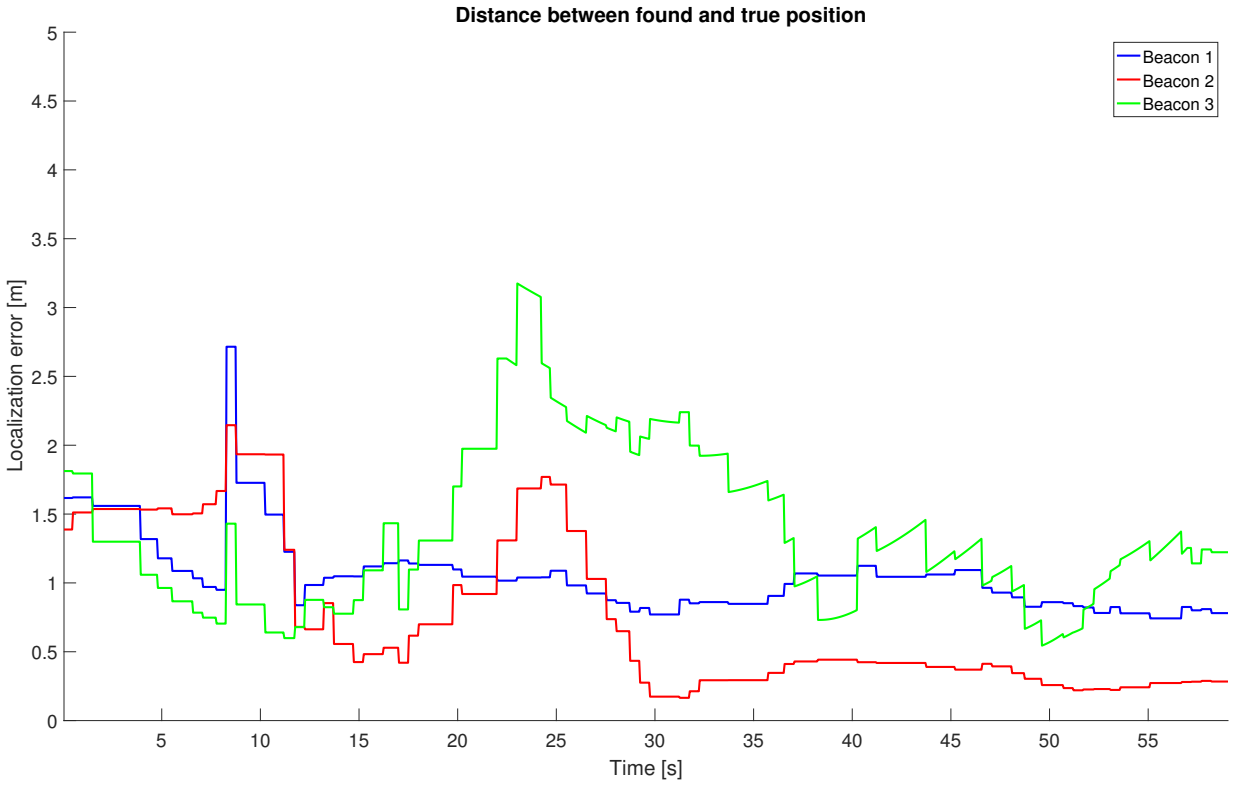

Figure 16: Distance between the true and found beacon position over time in this experiment

5.5.1 Analysis of results

The achieved precision of the algorithm in this experiment is worse than in the simulations, since the conditions were worse than what was simulated. The experiment localized the beacons in three dimensions instead of just two, the frequency of measurements was lower, the time of localization was shorter and there were obstacles and sources of signal reflection. In comparison with the localization experiments, presented in sections 5.3 and 5.4, the precision was comparable for beacon n. 1, slightly better for beacon n. 2 and worse for the dynamic beacon.

Obtained position of the beacon n. 2 showed approached the true position much faster than in previous experiments despite the slower sampling frequency (compare the error plots on Fig. 7, 11 and 16). This, together with better precision, is most probably caused by a higher number of MAVs and consequently a higher number of receivers. Localization of beacons number 1 and number 3 achieved worse results. The localization error of beacon 1 might have decreased further if the experiment lasted longer as the plot on Fig. 16 suggests. Slower localization is probably caused by a slower sampling rate and possibly also higher noise values. Beacon n. 1 has also been used from the beginning of this work

for testing and all the experiments (both documented and undocumented), which means that its remaining battery capacity has been lower than in case of the other beacons. This might have worsened its characteristics. Another influence which might have negatively impacted the localization is the dynamic obstacle, introduced in the system by the UGV. The aluminum construction on the UGV (as seen on Fig. 14) may have influenced the signal propagation in unpredictable ways. Localization error of beacon n. 3 (the dynamic beacon) includes some oscillations and it has the worst result from all three beacons at the end of the experiment. Since the aluminum frame on which the beacon was placed is conductive and it was not grounded, it could have acted as an antenna with unknown characteristics – namely directionality and gain. The oscillations in the localization error suggest that the characteristics of the beacon n. 3 changed with its position. This implies some directionality of the transmitter, which might be caused by the aluminum frame. Directionality of the beacons themselves is an unknown characteristic as well and will be examined in future work. The mean error of the dynamic beacon over the duration of the experiment was 1.37 m.

The signal range has been significantly shorter than in the other experiments with similar setups. The beacons had to be set to a state with higher transmitted power (and longer period between advertisement packets) in order to be detected by all the MAVs. The reason for this can be speculated and experimentally validating these speculations will be a part of future work on this project. Absorption of a significant part of transmitted power by the floor as proposed in conclusion of the first experiment, where signal range has been a problem as well, can be ruled out in case of this experiment. Other experiments proved that this effect is insignificant when the beacon and the receiver are placed higher above ground, which has been applied here (compare results in sections 5.1 and 5.2). An explanation of the shorter range might be a significantly higher level of signal noise than in the other experiments, causing the BLE advertisement packets to have too low SNR to be recognized by the receivers. This may be a result of a higher number of transmitters in the area, which increased the noise levels. There were three BLE beacons, three RC transmitters controlling the MAVs, and three notebooks connected to WiFi, all of which operated at the same frequency as the BLE technology (2.45 GHz), as opposed to just one BLE beacon, one (or none) RC transmitter and one (or none) WiFi connected notebook in the other experiments. The increased level of signal noise may also explain the worse precision and slower convergence of localized position to the true beacon position of beacons 1 and 3.

Finally, as was demonstrated in the previous experiments (specifically in sections 5.2 and 5.3), RSSI measurements of the BLE technology are very noisy in indoor environments and sensitive to obstacles causing signal reflections. Because the experiment took place indoors in a relatively small room (see Figure 13), this can not be neglected and it has surely negatively affected the results.

5.5.2 Conclusion

In general, the results showed that even under non-ideal conditions the algorithm can give relatively good results and also highlighted the weaknesses of the algorithm and the BLE technology. The algorithm can cope with dynamic beacons and dynamic obstacles to a certain degree, but the precision and speed of localization is negatively affected. Too many devices transmitting at the same frequency in the same area can cause the RSSI measurements to be more noisy. The main flaw of this experiment is that its duration was too short and it failed to show if the localization errors would continue converging to smaller values. Unfortunately this flaw has been identified too late to be corrected, but it will be avoided in future experiments.

5.6 Experiments summary

Experiments, described in this section, have shown that the algorithm, proposed in this thesis (see section 3), together with the used BLE technology can localize beacons robustly. Using a formation of three static MAVs, two beacons have been localized in three dimensions with a precision of 0.28 m and 0.78 m in one minute. Using a single moving MAV, two beacons have been localized in three minutes with a precision of 0.48 m and approximately 1.4 m. A moving beacon with speed $2\,\mathrm{m\,s^{-1}}$ has been localized by a formation of three static MAVs for one minute with a mean error of 1.37 m and progress of the error indicated further convergence to a smaller value in a longer experiment. The conditions affecting precision and speed of the localization are namely obstacles such as walls, columns, people or furniture, the number of MAVs/receivers, height of the beacon and receivers above ground, strength of the transmitted signal and frequency of transmitting the BLE advertisement packets. Other possible influences include the MAV trajectory, number of devices transmitting at the same frequency as the BLE beacons in the area, directionality and battery status of the beacons/transmitters and other sources of noise, which remain unknown.

Future experiments will include measuring signal strength in several defined positions around a beacon to determine its directionality, measuring beacon signal properties with a number of other 2.45 GHz transmitters in the area and measuring signal properties of a beacon with different states of the battery and finally a longer lasting large scale experiment in outdoor environment with less obstacles and walls, with a larger search area and moving MAVs.

6 Conclusion and future work

6.1 Conclusion

An algorithm for locating RF transmitters from position and range measurements using a formation of mobile robots with compatible receivers has been proposed and examined in this work. It is based on the Extended Kalman Filter and Log-Normal signal propagation model. The algorithm is described in section 3. The system model, together with the Log-Normal model, are described in section 2. The primary target application is finding RFID beacons in 3D environment with a formation of MAVs.

Simulation, presented in Section 4, has shown that the algorithm should be able to locate the beacons with a satisfactory precision. The average localization error was less than 0.25 m using a simulation set up that reflects the physical model and preliminary hardware experiments. The simulation showed that a precision difference when using the UKF and the EKF is minimal (less than 1 cm), but the speed advantage of the EKF is over 91%, which is why the EKF has been chosen for the rest of this work. The proposed algorithm should be sufficiently fast to be used on the MAV onboard computers in realtime This opens new interesting options to improve the algorithm by adjusting the search trajectory or other parameters of the algorithm during the mission. The maximal localization error in the simulation was relatively large (more than 2 m) and although 95% of resulting errors are smaller than 0.65 m, the occasional large error is a problem, which should be addressed in future work on this project.

Five experiments presented in Section 5 have been conducted. The first two showed that the BLE technology is usable for this application, but also defined the limitations of the technology. Namely the RSSI readings in indoor areas are very noisy and the relation between RSSI and transmitter/receiver distance is very inconsistent due to obstacles and reflections. Also the signal range is very limited if the transmitter and receiver are not at least a few centimetres above ground. The following two experiments proved that the approach described in section 3 works for localizing a beacon even with only one MAV. They again showed the limitations of the technology, as the resulting localization error was much larger when there was a disturbance in the form of a strong signal reflection from a concrete column. Finally, the last experiment showed how the algorithm works with more MAVs and how it performs with a moving beacon and a dynamic obstacle. The best result was an error of 0.28 m in the experiment with three MAVs, where the beacon has been localized with this precision in less than a minute. This is close to the expected precision under good conditions 0.25 m, as suggested by the simulation. The worst result was a 1.22 m final error with the dynamic beacon. This corresponds well with the simulation, considering that the experiments have been done in worse conditions (disturbances like reflections and obstacles have not been simulated) and the simulation has been done only in two dimensions.

6.2 Future work

Future work will focus on determining effects of RSSI measurement disturbances, like transmitter battery state, transmitter directionality, or height of transmitter and receiver, and ideally exploring a way to eliminate them or incorporate them into the system model and the algorithm. A longer lasting experiment to examine how the algorithm behaves in better conditions (in outdoor environment with less obstacles and walls) with a larger search area and moving MAVs would be the next step when continuing in this work. In outdoor locations, a variation of self-localization techniques of the MAVs could be used. For example, GPS combined with the onboard odometry and with the formation control ([2]) using optical detection of paper targets ([14]) carried on the MAVs (as was mentioned in the introduction, section 1). This could enable searching even large areas without integrating a position error from the odometry. Sensor fusion would become an even more important problem with this approach.

Improvement of the localization algorithm might be desirable, Especially finding a more robust algorithm for estimating the initial state for the KF, or incorporating knowledge about trajectory, search area and the area already covered by the MAVs into the algorithm. Including the non-constant time step, caused by the fact that the beacons may not always be in range of all receivers, should improve the localization, especially on larger areas. Further development could also include implementing the algorithm on onboard computers of the MAVs and running it in realtime, using the acquired information to dynamically adapt the MAV trajectory to improve the localization. Using a technology better than BLE, which would be less susceptible to RSSI disturbances, could significantly improve the localization and this option will be reviewed in future work.

References

[1] M. Saska, T. Krajnik, V. Vonasek, Z. Kasl, V. Spurny, and L. Preucil. Fault-Tolerant Formation Driving Mechanism Designed for Heterogeneous MAVs-UGVs Groups. *Journal of Intelligent and Robotic Systems*, 73(1-4):603–622, 2014.

[2] M. Saska, V. Vonasek, T. Krajnik, and L. Preucil. Coordination and Navigation of Heterogeneous MAV–UGV Formations Localized by a ḧawk-eye¨-like Approach Under a Model Predictive Control Scheme. *International Journal of Robotics Research*, 33 (10):1393–1412, 2014.

[3] Daan Scheerens. Practical indoor localization using bluetooth. Master's thesis, University of Twente, 2012.

[4] Timothy M. Bielawa. Position location of remote bluetooth devices. Master's thesis, Virginia Polytechnic Institute and State University, 2005.

[5] Viacheslav Filonenko, Charlie Cullen, and James Carswell. Asynchronous ultrasonic trilateration for indoor positioning of mobile phones. In *Web & Wireless*, 2012.

[6] Hyuk Lim, Lu-Chuan Kung, Jennifer C. Hou, and Haiyun Luo. Zero-configuration indoor localization over ieee 802.11 wireless infrastructure. *Wireless Networks*, 2010.

[7] Joseph J. LaViola Jr. A comparison of unscented and extended kalman filtering for estimating quaternion motion. In *American Control Conference*, 2003.

[8] Mathieu St-Pierre and Denis Gingras. Comparison between the unscented kalman filter and the extended kalman filter for the position estimation module of an integrated navigation information system. In *Intelligent Vehicles Symposium, IEEE*, 2004.

[9] M. Saska, T. Baca, J. Thomas, J. Chudoba, L. Preucil, T. Krajnik, J. Faigl, G. Loianno, and V. Kumar. System for deployment of groups of unmanned micro aerial vehicles in GPS-denied environments using onboard visual relative localization. *Autonomous Robots. First online.*, 2016.

[10] Tomáš Báča. Model predictive control of micro aerial vehicle using onboard microcontroller. Master's thesis, Czech Technical University in Prague, 2015.

[11] Tomáš Báča and Martin Saska. Embedded model predictive control of micro aerial vehicles. In *International Conference on Methods and Models in Automation and Robotics*, 2016.

[12] M. Saska, Z. Kasl, and L. Preucil. Motion Planning and Control of Formations of Micro Aerial Vehicles. In *Proceedings of The 19th World Congress of the International Federation of Automatic Control (IFAC)*. IFAC, 2014.

[13] T. Krajnik, M. Nitsche, J. Faigl, P. Vanek, M. Saska, L. Preucil, T. Duckett, and M. Mejail. A practical multirobot localization system. *Journal of Intelligent & Robotic Systems*, 76(3-4):539–562, 2014.

[14] J. Faigl, T. Krajnik, J. Chudoba, L. Preucil, and M. Saska. Low-Cost Embedded System for Relative Localization in Robotic Swarms. In *Proceedings of 2013 IEEE International Conference on Robotics and Automation (ICRA)*, 2013.

[15] M. Saska, J. Chudoba, L. Preucil, J. Thomas, G. Loianno, A. Tresnak, V. Vonasek, and V. Kumar. Autonomous Deployment of Swarms of Micro-Aerial Vehicles in Cooperative Surveillance. In *Proceedings of 2014 International Conference on Unmanned Aircraft Systems (ICUAS)*, 2014.

[16] M. Saska, V. Vonásek, J. Chudoba, J. Thomas, G. Loianno, and V. Kumar. Swarm distribution and deployment for cooperative surveillance by micro-aerial vehicles. *Journal of Intelligent & Robotic Systems. First online.*, 2016.

[17] Anja Bekkelien. Bluetooth indoor positioning. Master's thesis, University of Geneva, 2012.

[18] Michael Quan Eduardo Navarro, Benjamin Peuker. Wi-fi localization using rssi fingerprinting. 2011.

[19] Javier Rodas, Tiago M. Fernández, Daniel I. Iglesia, and Carlos J. Escudero. Multiple antennas bluetooth system for rssi stabilization. In *Wireless Communication Systems. ISWCS. 4th International Symposium on*, 2007.

[20] S. J. Julier and J. K. Uhlmann. A new extension of the kalman filter to nonlinear systems. *Proc. of AeroSense: The 11th Int. Symp. on Aerospace/Defence Sensing, Simulation and Controls*, 1997.

[21] Fredrik Gustafsson and Gustaf Hendeby. Some relations between extended and unscented kalman filters. *IEEE Transactions on Signal Processing*, 2012.

[22] Johannes Schmid, Frederik Beutler, Benjamin Noack, Uwe D. Hanebeck, and Klaus D. Müller-Glaser. An experimental evaluation of position estimation methods for person localization in wireless sensor networks. In *Proceedings of the 8th European conference on Wireless sensor networks*, 2011.

Appendix A CD Content

Names of all root directories on the CD and their descriptions are listed in Table 4. In each of these directories you will find a README file with a description of files in the directory.

Directory name	**Description**
thesis	Bachelor's thesis in pdf format
thesis/source	latex sources for the thesis
Cpp	C++ source codes
MATLAB/experiments	MATLAB source codes and data from experiments
MATLAB/simulation	MATLAB source codes and data from simulation
videos	videos from experiments

Table 4: CD Content

Appendix B List of abbreviations

Abbreviations used in this project are listed in the Table 5.

Abbreviation	Meaning
AP	access point
BLE	bluetooth low energy
CPU	central processing unit
EKF	extended kalman filter
GPS	global positioning system
ID	identifier
KF	kalman filter
MAV	micro aerial vehicle
MPC	model predictive control
OS	operation system
PC	personal computer
RC	radio controlled
RF	radio frequency
RFID	radio frequency identification
RSS	received signal strength
RSSI	received signal strength indication
SNR	signal to noise ratio
UGV	unmanned ground vehicle
UKF	unscented kalman filter
USB	universal serial bus
WiFi	wireless standard IEEE 802.11

Table 5: Lists of abbreviations